

*An Introduction to*  
**COSMOLOGY**  
*and*  
**PARTICLE PHYSICS**

**Rosa Domínguez-Tenreiro**

Departamento de Física Teórica  
Universidad Autónoma de Madrid  
Cantoblanco, 28049-Madrid, Spain

**Mariano Quirós**

Instituto de Estructura de la Materia  
Consejo Superior de Investigaciones Científicas  
Serrano 119, 28006-Madrid, Spain

 **World Scientific**  
*Singapore • New Jersey • Hong Kong*

*Published by*

**World Scientific Publishing Co, Pte. Ltd.**  
P.O. Box 128, Farrer Road, Singapore 9128

*U. S. A. office:* World Scientific Publishing Co., Inc.  
687 Hartwell Street, Teaneck NJ 07666, USA

**Library of Congress Cataloging-in-Publication Data**

Domínguez-Teneiro, Ross.  
An introduction to cosmology and particle physics.

Includes bibliographies.

1. Cosmology. 2. Particles (Nuclear physics)  
3. Nuclear astrophysics. I. Quirós, M. II. Title.

QB981.D66 1988 523.1 88-263

ISBN 9971-50-306-9

ISBN 9971-50-309-3 (pbk)

**An Introduction to Cosmology and Particle Physics**

Copyright © 1988 by World Scientific Publishing Co Pte Ltd.

*All rights reserved. This book, or parts thereof, may not be reproduced in any form or by any means, electronic or mechanical, including photocopying, recording or any information storage and retrieval system now known or to be invented, without written permission from the Publisher.*

ISBN 9971-50-306-9

ISBN 9971-50-309-3 (pbk)

Printed in Singapore by General Printing Services Pte. Ltd.

## FOREWORD

This book is based on a series of lectures, sponsored by the Grupo Interuniversitario de Física Teórica (GIFT), given at the Universidad Autónoma de Madrid (UAM) during the spring of 1986 and on an advanced course for graduate students currently in progress at the UAM. Its level is introductory and it is addressed to graduate students in Cosmology and Theoretical High Energy Physics.

We would like to thank Gordy Kane, José Luis Sanz and Nicola Vittorio for a critical reading of different parts of the manuscript and many useful suggestions.

One of the authors (R.D.-T.) wants to thank Angeles Díaz and Gustavo Yepes for collaborations and fruitful discussions about some of the subjects treated in this book. The other of the authors (M.Q.) wants to express his deep thankfulness to his collaborators John Ellis, Kari Enqvist, Costas Kounnas, Dimitri Nanopoulos, Keith Olive and Marc Srednicki for enjoyable and unforgettable work done together.

We also acknowledge the Astrophysical Journal, Nuclear Physics, Physical Review, Quarterly Journal of the Royal Astronomical Society and Science as the original location of publication of some of the figures reproduced in this book and the Patrimonio Artístico Nacional of Spain for its kind permission to reproduce the figure on the cover.

Finally the authors would like to express their gratitude to Ana Montero Cuéllar for her careful typing of the manuscript.

Rosa Domínguez-Tenreiro

Mariano Quirós





## CONTENTS

FOREWORD .....	v
CHAPTER 1. THE STANDARD COSMOLOGICAL MODEL .....	1
1.1 The Cosmological Principle .....	3
1.2 Einstein's equations .....	6
1.3 Some results from Relativistic Kinetic Theory .....	16
1.4 Thermal history of the universe .....	19
References 1 .....	30
CHAPTER 2. DETERMINATION OF THE COSMOLOGICAL PARAMETERS .....	31
2.1 The red-shift .....	32
2.2 The determination of the Hubble constant and the deceleration parameter .....	34
2.3 Determination of the density parameter .....	41
References 2 .....	51
CHAPTER 3. THE COSMIC MICROWAVE BACKGROUND .....	53
3.1 The spectrum of the cosmic microwave background .....	54
3.1.1 Standard cosmological model predictions .....	54
3.1.2 Observations .....	59
3.2 Angular distribution of the microwave background .....	61
radiation	
3.2.1 The peculiar velocity of the observer .....	61
3.2.2 The horizon problem .....	64
3.2.3 Observations .....	66
References 3 .....	70

<b>CHAPTER 4. THE STANDARD BIG-BANG NUCLEOSYNTHESIS .....</b>	<b>71</b>
4.1 The primordial nucleosynthesis process in standard cosmologies .....	72
4.2 Predicted abundances and their uncertainties .....	79
4.3 Observed abundances .....	84
4.3.1 Deuterium .....	84
4.3.2 Helium 3 .....	88
4.3.3 Helium 4 .....	89
4.3.4 Lithium 7 .....	93
4.4 Primordial abundances and consistency theory/ astronomical data .....	94
References 4 .....	101
 <b>CHAPTER 5. THE LARGE SCALE STRUCTURE FORMATION .....</b>	 <b>103</b>
5.1 Characteristic masses .....	104
5.1.1 Jeans mass for a photon, baryon, electron and massless neutrino gas .....	105
5.1.2 Silk mass .....	106
5.1.3 Jeans mass for massive collisionless particles ..	109
5.2 Observations .....	118
5.3 Linear theory of perturbations to FRW model .....	128
5.3.1 Equations for the perturbations .....	129
5.3.2 Ideal fluid .....	132
5.3.3 Collisionless gas .....	135
5.3.4 Photon gas near the recombination .....	137
5.3.5 General resolution method and normalization .....	138
5.4 Transfer functions and coherence lengths .....	143
5.5 Cosmic microwave background anisotropies .....	147
5.5.1 Small scale anisotropies .....	148
5.5.2 Large scale CMB fluctuations: gauge invariant formalism .....	150
5.5.3 Results .....	153
5.6 Large scale peculiar velocities .....	155
5.7 N-body simulations .....	157
5.8 Biased structure formation scenario .....	162
References 5 .....	165

<b>CHAPTER 6. SOME COSMOLOGICAL LIMITS ON THE PARAMETER OF EXOTIC PARTICLES .....</b>	<b>168</b>
6.1 Evolution of the concentration of massive particles ....	169
6.2 Light element yields with non-standard particles content .....	177
6.3 Distortion of the cosmic background radiation by decaying particles .....	182
6.4 Cosmological bounds on massive neutrinos .....	186
6.4.1 The mean density of the universe .....	186
6.4.2 Massive neutrinos and light element abundances ..	188
6.4.3 Cosmic microwave background distortions .....	192
6.5 Cosmological limits on the microphysical parameters of light particles .....	192
6.5.1 Bounds on the number of weakly interacting particles .....	192
6.5.2 Bounds on the mass of light neutrinos .....	195
6.5.3 The chemical potential of neutrinos .....	196
6.6 Cosmological limits for supersymmetric particles .....	200
References 6 .....	207
 <b>CHAPTER 7. FINITE TEMPERATURE EFFECTIVE POTENTIAL AND PHASE TRANSITIONS .....</b>	 <b>209</b>
7.1 General formalism .....	210
7.2 Finite temperature Green functions .....	213
7.2.1 Spinless fields .....	213
7.2.2 Fermion fields .....	216
7.2.3 Feynman rules .....	217
7.3 Finite temperature effective potential for spinless particles .....	218
7.4 Finite temperature effective potential for fermion fields .....	223
7.5 Finite temperature effective potential for gauge fields .....	229
7.6 Finite temperature effective potential for a general theory .....	232

7.7	Phase transitions in field theories .....	234
7.7.1	A toy model .....	235
7.7.2	SU(5) Coleman-Weinberg potential .....	239
	References 7 .....	243
CHAPTER 8. PROBLEMS OF THE STANDARD BIG-BANG MODEL .....		244
8.1	Introduction .....	244
8.2	The flatness (oldness) problem .....	245
8.3	The horizon problem .....	249
8.4	A solution to the flatness and horizon problems: inflationary universe scenarios .....	254
8.4.1	Inflation solves the horizon problem .....	257
8.4.2	Inflation solves the flatness problem .....	259
8.5	Other problems of the standard cosmological model .....	262
8.5.1	Small-scale inhomogeneity and galaxy formation .....	262
8.5.2	The domain wall problem .....	264
8.5.3	The baryon number of the universe .....	265
8.5.4	The cosmological constant problem .....	270
8.6	Baryogenesis .....	272
8.6.1	The standard out-of-equilibrium decay scenario ..	275
8.6.2	Baryogenesis in Grand Unified Theories .....	282
	References 8 .....	294
CHAPTER 9. THE DYNAMICS OF INFLATION .....		297
9.1	Introduction .....	297
9.2	The Hawking temperature .....	300
9.3	The dynamics of first-order phase transitions .....	308
9.3.1	Semiclassical theory of false vacuum decay .....	309
9.3.2	Gravitational effects on false vacuum decay .....	322
9.3.3	The Hawking-Moss transition .....	329

9.4	The slow rollover regime .....	336
9.5	Coherent field oscillations and reheating .....	342
9.6	Energy density perturbations and galaxy formation .....	350
	References 9 .....	366
CHAPTER 10. INFLATIONARY MODELS .....		368
10.1	Nearly Coleman-Weinberg models .....	368
10.2	Inflation cries out for supersymmetry .....	377
10.3	Primordial inflation in supergravity .....	380
	10.3.1 Inflationary models in minimal supergravity .....	386
	10.3.2 Inflationary models in no-scale supergravity .....	392
10.4	Chaotic inflation .....	406
10.5	Double inflation .....	411
	References 10 .....	420
APPENDIX .....		422
	Conversion factors in natural units and some cosmological constants	



*An Introduction to*  
**COSMOLOGY**  
*and*  
**PARTICLE PHYSICS**





# CHAPTER 1

## THE STANDARD COSMOLOGICAL MODEL

The purpose of Physical Cosmology is to study the universe from a global point of view and to describe the physical processes which have occurred throughout its evolution and which have observable consequences nowadays.

Astronomical observations are not exhaustive and they provide us with information about the universe which is limited, both spatially and temporarily. The models describing the universe and its evolution are then necessarily based upon an extrapolation of physical theories whose validity has only been locally tested out. This extrapolation, known as the Relativity Principle, states that physical laws are everywhere the same and at all times.

Given the spatial scales in play, gravitation is one basic tool to build up a cosmological model. The gravitation theory to be used is

the first choice to be made. Solar System and binary pulsar data largely suggest that Einstein's General Relativity describes adequately well the gravitational interaction at present times<sup>(1)</sup>. However, there exists a set of alternative gravitation theories which tend to General Relativity in some limits, and it has not yet been proven that they should be excluded in describing the early universe<sup>(1)</sup>.

The standard cosmological model is based upon a set of hypotheses which make it the simplest global description of the universe. The first of them is to assume that General Relativity, whose field content is minimum among the metric theories, is the correct gravitation theory. The second assumption is that hypersurfaces of constant time are homogeneous and isotropic (Cosmological Principle). This is the maximum symmetry compatible with evolution.

The other ingredient of a cosmological model is the particle content of the universe. In the standard cosmological model it is assumed that these particles and their interactions correspond to the standard particle physics model, which has been tested in terrestrial accelerators up to energies of the order of 100 GeV. Statistical Physics is supposed to describe the behavior of collections of big numbers of these particles.

With these simple and, to some extent, natural hypotheses, the evolution of the universe can be modelled, except for some parameters which have to be determined observationally.

In this first Chapter we will introduce the standard

cosmological model, which will be the framework to study, in forthcoming Chapters, the light element synthesis and the large scale structure formation. The other cosmologically important observations, namely the red-shift of spectral lines of distant objects and the cosmic microwave background, are well interpreted in the framework of the standard model, but also of any other model which predicts expansion or a hotter phase in the evolution of the universe, respectively.

The following notation will be used along this book: greek indices run from 0 to 3; latin indices take the values 1, 2 and 3;  $\dot{A}$  stands for time derivative and  $A_{,\mu} = \partial A / \partial x^\mu$ .

## 1.1 THE COSMOLOGICAL PRINCIPLE

The Cosmological Principle states that the three-spaces of constant time are maximally symmetric, that is, homogeneous and isotropic, at all times.

The Cosmological Principle is founded on the Copernican Principle, which states that we are not privileged observers and, consequently, it can be expected that the universe observed from any other point looks the same as observed from the Earth. This assumption, together with that of the isotropy of the universe as observed from the Earth, implies the Cosmological Principle at the present time, because any space that is isotropic about every point is also homogeneous<sup>(2)</sup>. The Relativity Principle then ensures that it

applies at all times.

These considerations which were first introduced as an acceptable simplifying mathematical hypothesis, have been observationally confirmed to some extent. We quote the following observations:

i) The cosmic microwave isotropy at any scale: only a dipole component has been detected, which can be interpreted in terms of the peculiar motion of the Local Group of galaxies. Small scale anisotropies in the cosmic microwave temperature are bounded by:

$$\Delta T/T \lesssim 10^{-4} \quad (1.1)$$

and on some scales by:

$$\Delta T/T \lesssim 3 \times 10^{-5} \quad (1.2)$$

(see Chapter 3).

ii) The light element abundances, which with the help of a model of the anisotropy evolution from light element formation at  $T \approx 10^9 \text{K}$  up to the present, enable us to limit the large scale anisotropy by less than one part in  $10^8$  (3).

iii) The two point galaxy correlation function  $\xi_g(r)$  shows a universal behavior, independently from the catalogue<sup>(4)</sup> (see eq. (5.36)). This is an isotropy test (different catalogues consist of sets of galaxies taken from different directions).

A mathematical consequence of the Cosmological Principle is the existence of a coordinate system in which the metric of space-time takes the form<sup>(2)</sup>:

$$ds^2 \equiv g_{\mu\nu} dx^\mu dx^\nu = dt^2 - R^2(t) d\sigma^2 \quad (1.3)$$

where  $g_{\mu\nu}$  are the components of the metric tensor and  $d\sigma^2$  is the three-space metric and is time independent. It can be written in the form:

$$d\sigma^2 \equiv -\tilde{g}_{ij} dx^i dx^j = \frac{dr^2}{1-kr^2} + r^2(d\theta^2 + \sin^2\theta d\phi^2) \quad (1.4)$$

with  $k$  the curvature constant, which represents the sign of the intrinsic curvature of the maximally symmetric three-spaces, and takes the values  $k = 1, 0$  and  $-1$ . This form of the metric results only from symmetry considerations and is known as the Robertson-Walker metric (R-W). In these kind of metrics only one dynamical function,  $R(t)$ , has to be determined by means of the field equations of the gravitation theory, in our case Einstein's equations.

If  $k=1$ , the three-spaces are finite, with proper volume given by:

$${}^3V = 2\pi R^3(t) \quad (1.5)$$

and  $R(t)$  can then be interpreted as the "radius" of the universe. If  $k=0$  or  $-1$ , no such interpretation is possible. However,  $R(t)$  still gives a measure of the scale of the geometry in the three-space, and is in any case termed the cosmic scale factor.

## 1.2 EINSTEIN'S EQUATIONS

The considerations about the form of the metric of space-time made in the previous Section are now to be completed by the study of its dynamics by means of Einstein's equations.

Let us first briefly review some results from Differential Geometry to be used in this Section. Given a space with metric  $g_{\mu\nu}$ , the affine connection or Christoffel symbols are given by

$$\Gamma_{\rho\lambda}^{\mu} \equiv \frac{1}{2} g^{\mu\nu} \left[ g_{\rho\nu,\lambda} + g_{\lambda\nu,\rho} - g_{\rho\lambda,\nu} \right] = \Gamma_{\lambda\rho}^{\mu} \quad (1.6)$$

where  $g^{\mu\nu}$  is the inverse of the metric matrix

$$g^{\mu\nu} g_{\mu\lambda} = \delta_{\lambda}^{\nu} \quad (1.7)$$

and the second equality in eq. (1.6) follows from the symmetry of the metric.

The covariant derivative of the contravariant components of a tensor field is defined by means of the Christoffel symbols:

$$T^{\nu\rho\dots}{}_{;\mu} \equiv T^{\nu\rho\dots}{}_{,\mu} + \Gamma_{\mu\lambda}^{\nu} T^{\lambda\rho\dots} + \Gamma_{\mu\lambda}^{\rho} T^{\nu\lambda\dots} + \dots \quad (1.8)$$

and for the covariant components:

$$T_{\nu\rho\dots}{}_{;\mu} \equiv T_{\nu\rho\dots}{}_{,\mu} - \Gamma_{\mu\nu}^{\lambda} T_{\lambda\rho\dots} - \Gamma_{\mu\rho}^{\lambda} T_{\nu\lambda\dots} - \dots \quad (1.9)$$

with evident extensions to components of mixed type.

The Riemann curvature tensor is also defined in terms of the affine connection:

$$R^{\lambda}_{\mu\nu\rho} \equiv \Gamma^{\lambda}_{\mu\nu,\rho} - \Gamma^{\lambda}_{\mu\rho,\nu} + \Gamma^{\sigma}_{\mu\nu} \Gamma^{\lambda}_{\rho\sigma} - \Gamma^{\sigma}_{\mu\rho} \Gamma^{\lambda}_{\nu\sigma} \quad (1.10)$$

The Ricci tensor is obtained by contracting the above expression in the indices  $\lambda$  and  $\nu$ :

$$R_{\mu\rho} \equiv R^{\lambda}_{\mu\lambda\rho} = \Gamma^{\lambda}_{\mu\lambda,\rho} - \Gamma^{\lambda}_{\mu\rho,\lambda} + \Gamma^{\sigma}_{\mu\lambda} \Gamma^{\lambda}_{\rho\sigma} - \Gamma^{\sigma}_{\mu\rho} \Gamma^{\lambda}_{\lambda\sigma} \quad (1.11)$$

whose trace is the curvature scalar  $R_c$ :

$$R_c \equiv g^{\mu\nu} R_{\mu\nu} \quad (1.12)$$

It can be shown that the Ricci tensor for a maximally symmetric subspace of dimension  $N$  is given by:

$$R_{ab} = \frac{1}{N} R_c g_{ab} \quad a, b = 1, \dots, N \quad (1.13)$$

For the three-spaces we have:

$$\tilde{R}_{ij} = 2k \tilde{g}_{ij} \quad (1.14)$$

where, according to eq. (1.4):

$$\tilde{g}_{rr} = \frac{-1}{1-kr^2} \quad (1.15)$$

$$\tilde{g}_{\theta\theta} = -r^2 \quad (1.16)$$

and

$$\tilde{g}_{\phi\phi} = -r^2 \sin^2 \theta \quad (1.17)$$

are the non-zero elements of the metric for the maximally symmetric three-spaces. We see that

$$\tilde{R}_c = 6k \quad (1.18)$$

and hence the interpretation of  $k$  given in the previous Section.

Einstein's equations can be written as:

$$R_{\mu\nu} - \Lambda g_{\mu\nu} = -8\pi G (T_{\mu\nu} - \frac{1}{2} g_{\mu\nu} T^\lambda_\lambda) \quad (1.19)$$

where  $\Lambda$  is the cosmological constant and  $G$  is Newton's gravitational constant.  $T_{\mu\nu}$  is the energy-momentum tensor, which has to be maximally form-invariant on the hypersurfaces of constant time. This requires that  $T_{\mu\nu}$  has a perfect fluid form:

$$T_{\mu\nu} = -Pg_{\mu\nu} + (\rho + P)u_\mu u_\nu \quad (1.20)$$

where  $u^\mu$  is the mean velocity of the fluid

$$\begin{aligned} u^0 &= 1 \\ u^i &= 0 \\ u^\alpha u_\alpha &= 1 \end{aligned} \quad (1.21)$$



that is, the universe content is, on average, at rest in our coordinate system.  $P(t)$  and  $\rho(t)$  are the pressure and the energy density of the isotropic fluid, which are to be calculated from Kinetic Theory.

In order to write Einstein's equations (1.19) explicitly, the Ricci tensor for the R-W metric has to be computed by means of eq. (1.11). The non-zero components are:

$$R_{00} = 3 \frac{\ddot{R}}{R} \quad (1.22)$$

$$R_{ij} = (R\ddot{R} + 2\dot{R}^2 + 2k) \tilde{g}_{ij} \quad (1.23)$$

The field equations follow from eqs. (1.20) to (1.23). The 0-0 term gives:

$$3\ddot{R} = -4\pi G(\rho + 3P)R + \Lambda R \quad (1.24)$$

The spatial components then lead to only one equation:

$$R\ddot{R} + 2\dot{R}^2 + 2k = 4\pi G(\rho - P)R^2 + \Lambda R^2 \quad (1.25)$$

Removing  $\ddot{R}$ , we obtain:

$$H^2 \equiv \left[ \frac{\dot{R}}{R} \right]^2 = \frac{8\pi G}{3} \rho + \frac{1}{3} \Lambda - \frac{k}{R^2} \quad (1.26)$$

which defines the Hubble parameter  $H$ .

The energy-momentum tensor satisfies the conservation equation:

$$T^{\mu\nu}_{;\mu} = 0 \quad (1.27)$$

which can be deduced from Einstein's equations through the Bianchi identities

$$R_{\lambda\mu\nu\sigma;\eta} + R_{\lambda\mu\eta\nu;\sigma} + R_{\lambda\mu\sigma\eta;\nu} = 0 \quad (1.28)$$

where

$$R_{\lambda\mu\nu\sigma} = g_{\lambda\eta} R^{\eta}_{\mu\nu\sigma} \quad (1.29)$$

For  $\nu=0$ , eq. (1.27) gives (energy conservation):

$$\dot{R}R^3 = \frac{d}{dt} \left[ R^3(\rho+P) \right] \quad (1.30)$$

or, equivalently:

$$\frac{d}{dR} (\rho R^3) = -3PR^2 \quad (1.31)$$

Once a state equation  $P = P(\rho)$  is given, eq. (1.31) determines the function  $\rho(R)$ , and then eq. (1.26) gives the time evolution of  $R$ , that is, the function  $R(t)$ . This determines all the dynamics of the universe. Cosmological models based on the R-W metric, in which  $R(t)$  is evaluated in this way, are known as Friedmann-Robertson-Walker (FRW) models<sup>(4)</sup>.

Some qualitative features of the evolution of the universe can be deduced without specifying the state equation. Two different situations arise, depending on the value of the cosmological constant:

i) In the standard cosmological model it is assumed that  $\Lambda=0$ .

In this case eq. (1.24) implies that  $\frac{\ddot{R}}{R} < 0$  as long as  $\rho + 3P$  is positive. Moreover  $R > 0$  by definition, and  $\dot{R}/R > 0$ , because we now see red-shifts and no blue-shifts (see Chapter 2). We conclude that  $R(t)$  is an increasing function of time at the present and that the  $R(t)$  versus  $t$  curve cuts the  $t$  axis at some finite time in the past, if Einstein's equations hold at every time. The zero instant,  $t = 0$ , is defined by:

$$R(0) = 0 \tag{1.32}$$

at which point the model has a singularity, and the age of the universe  $t_0$  is the time elapsed since then, and has a finite value.

On the other hand, eq. (1.31) requires that  $\rho$  decreases with increasing  $R$  at least as  $R^{-3}$ , if  $P$  is positive, and then eq. (1.26) implies that:

$$\dot{R}^2 \longrightarrow R^{-1} - k$$

when  $R \longrightarrow \infty$ . The consequences of this behavior in the future expansion depend on the  $k$  sign: If  $k = -1$ , then  $R(t) \longrightarrow t$  as  $t \longrightarrow \infty$  and the universe expands forever. If  $k = 0$ , then  $R(t) \longrightarrow t^a$ , with  $a < 1$  as  $t \longrightarrow \infty$ , and the universe expands indefinitely, but slower than for  $k = -1$ . If  $k = 1$ , the expansion stops ( $\dot{R} = 0$ ) at the time when:

$$\frac{8\pi G}{3} \rho - \frac{k}{R^2} = 0 \quad (1.33)$$

and then  $\dot{R}$  will take negative values, because  $\ddot{R} < 0$ . The universe recollapses and reaches, yet again, a singularity in a finite time in the future. We see that the future trends of the evolution of the universe are determined by the geometry of the three-spaces. If  $k = 1$ , the model is termed closed; if  $k = 0$ , we have a zero scalar curvature and the geometry is flat; if  $k = -1$  the model is open.

Eq. (1.26) can be written in the form:

$$\frac{k}{R^2} = H^2(\Omega - 1) \quad (1.34)$$

where the cosmological density parameter is defined by:

$$\Omega(t) \equiv \frac{\rho(t)}{\rho_c(t)} \quad (1.35)$$

and

$$\rho_c(t) \equiv \frac{3H^2(t)}{8\pi G} \quad (1.36)$$

is known as the critical energy density at time  $t$ .

Defining the deceleration parameter by:

$$q(t) \equiv - \frac{\ddot{R}(t)}{R(t)H^2(t)} \quad (1.37)$$

eq. (1.24) becomes at the present time (a zero subscript means present values of the dynamical functions):

$$q_0 = \frac{1}{2} \Omega_0 + \frac{4\pi G P_0}{H_0^2} \quad (1.38)$$

The present pressure of the universe is negligible (see Section 1.4). Eqs. (1.34), (1.35) and (1.38) give then the following equivalences:

$$k = 1 \iff \Omega > 1 \iff \rho > \rho_c \iff q_0 > \frac{1}{2} \quad (1.39)$$

$$k = 0 \iff \Omega = 1 \iff \rho = \rho_c \iff q_0 = \frac{1}{2} \quad (1.40)$$

$$k = -1 \iff \Omega < 1 \iff \rho < \rho_c \iff q_0 < \frac{1}{2} \quad (1.41)$$

That is, a closed (open) FRW universe with zero cosmological constant has a cosmological density parameter greater (smaller) than the unity and an energy density greater (smaller) than the critical density. This is the density of the flat models, which have a cosmological density parameter equal to unity. The geometry of the hypersurfaces of constant time are then determined by the content of the universe.

ii) Let us now consider the situation where  $\Lambda \neq 0$ . If, at some time:

$$\Lambda \gg -\frac{3k}{R^2} + 8\pi G\rho$$

then, according to eq. (1.26):

$$\left[ \frac{\dot{R}}{R} \right]^2 = \frac{\Lambda}{3} \quad (1.42)$$

which implies an exponential expansion (see Chapter 8)

$$R \propto \exp \left[ (\Lambda/3)^{1/2} t \right] \quad (1.43)$$

We know that the present expansion is not dominated by the  $\Lambda$  term. This requires that<sup>(5)</sup>:

$$\frac{\Lambda}{M_{Pl}^2} \lesssim 10^{-121} \quad (1.44)$$

where  $M_{Pl}$  is the Planck mass. This limit is not yet understood from the point of view of Particle Physics (see Chapter 8).

If  $\Lambda \neq 0$ , eq. (1.26) and (1.24) can be written as:

$$\frac{k}{R^2} = H^2(\Omega - 1) + \frac{\Lambda}{3} \quad (1.45)$$

$$q = \frac{\Omega}{2} + \frac{4\pi G P}{H^2} - \frac{\Lambda}{3H^2} \quad (1.46)$$

which means that the equivalences (1.39), (1.40) and (1.41) do not hold now.

A particular case of the closed  $\Lambda \neq 0$  models is when  $\Lambda = \Lambda_E \equiv 4\pi G(\rho+3P)$  and  $R^{-2} = R_E^{-2} \equiv 4\pi G(\rho+P)$ . Then  $\dot{R} = 0$  and  $\ddot{R} = 0$ . This is Einstein's static model in which no expansion occurs. The cosmological constant was historically introduced to avoid the universe expansion characteristic of the  $\Lambda = 0$  models, before the interpretation of the galaxy red-shifts as a cosmological Döppler effect was well stated.

Bounds on the age of the universe can be derived from observations<sup>(6)</sup>. The age of the universe in the standard model can be calculated from eq. (1.26). For some particular state equations, an analytical solution can be found<sup>(2)</sup>:

$$t_u = f(\Omega_0) H_0^{-1} \quad (1.47)$$

i)  $P_0 = \rho_0/3$  . Then

$$f(\Omega_0) = (1 + \sqrt{\Omega_0})^{-1} \quad (1.48)$$

ii) If  $P_0 \ll \rho_0$  , then:

for  $k = 0$

$$f = \frac{2}{3} \quad (1.49)$$

for  $k = -1$

$$f(\Omega_0) = (1-\Omega_0)^{-1} - \frac{\Omega_0}{2} (1-\Omega_0)^{-3/2} \cosh^{-1} \left[ \frac{2}{\Omega_0} - 1 \right] \quad (1.50)$$

and for  $k = 1$

$$f(\Omega_0) = \frac{\Omega_0}{2} (\Omega_0-1)^{-3/2} \left[ \cos^{-1} \left[ \frac{2}{\Omega_0} - 1 \right] - \frac{2}{\Omega_0} (\Omega_0-1)^{1/2} \right] \quad (1.51)$$

In any case it is found that:

$$t_u < H_0^{-1} \quad (1.52)$$

### 1.3 SOME RESULTS FROM RELATIVISTIC KINETIC THEORY

It is generally assumed that at early times the particle content of the universe formed an ideal gas. The physical properties of this ideal gas can be derived from Relativistic Kinetic Theory. A review on this subject can be found in reference 7, here we will only sketch its main results and their cosmologically relevant consequences.

The key instrument in describing a population of particles of type  $i$  is its distribution function,  $N_i(p^\mu)$ , which gives the number density of such particles having four-momenta in a neighborhood of  $p^\mu$ . Its space-time variation is given by the Boltzmann equation, which in this framework reads:

$$L_i N_i = \sum_{\substack{j \dots \\ \ell m \dots}} \int \pi_j \dots \int \pi_\ell \pi_m \dots N_\ell N_m \dots (1 \pm N_i)(1 \pm N_j) \dots \\ W(\ell m \dots \rightarrow i j \dots) - N_i N_j \dots (1 \pm N_\ell)(1 \pm N_m) \dots W(i j \dots \rightarrow \ell m \dots) \\ \equiv C[N_i] \tag{1.53}$$

In this equation,  $L_i$  is the Liouville operator in General Relativity, which can be written as:

$$L_i \equiv p^\alpha \frac{\partial}{\partial x^\alpha} - \Gamma_{\alpha\beta}^\mu p^\alpha p^\beta \frac{\partial}{\partial p^\mu} \tag{1.54}$$

The right hand side or collision term of eq. (1.53) describes the  $N_i$  variations due to the  $i$  particle collisions.  $W(ab \dots \rightarrow cd \dots)$  is the elementary transition rate for the process  $a+b+\dots \rightarrow c+d+\dots$  and  $\pi_p$  is



the volume element in the phase space for particles of type p:

$$\pi_p = (2\pi)^{-3} \sqrt{-g} g_p |p_o|^{-1} d^3p \quad (1.55)$$

where  $g = \det(g_{\mu\nu})$  and  $g_p$  is the particle spin degeneracy. The momenta and the particle mass are related by:

$$m_p^2 = g_{\alpha\beta} p^\alpha p^\beta \quad (1.56)$$

The  $(1 \pm N_p)$  factors in the integrand of eq. (1.53) describe the stimulated emission (for bosons) or the Fermi suppression factor (for fermions) for outgoing particles. The upper sign in  $\pm$  refers to bosons and the lower one to fermions.

If the transition rate for the process  $i+j+\dots \leftrightarrow \ell+m+\dots$  is in either direction much greater than the net production rate of  $i$  particles,  $L_i N_i$ , then the solution of equation (1.53) is:

$$N_i(p^\mu, x^\lambda) = \left\{ \exp \left[ -\alpha_i(x^\lambda) - \beta_\mu(x^\lambda) p^\mu \right] \mp 1 \right\}^{-1} \quad (1.57)$$

This situation is known as thermal equilibrium, and then an average velocity  $u_\mu$  can be defined such that:

$$\beta_\mu = -\beta u_\mu \quad (1.58)$$

The cosmic gas is then isotropic with respect to observers who travel with velocity  $u_\mu$ , which requires that the energy-momentum tensor has the perfect fluid form (1.20). It can be calculated through the distribution function: ,

$$T_i^{\mu\nu} = \int \pi_i N_i(p^\rho, x^\lambda) p^\mu p^\nu \quad (1.59)$$

The current density of particles of class  $i$  can also be obtained by means of  $N_i$ :

$$J_i^\mu = \int \pi_i N_i(p^\rho, x^\lambda) p^\mu = n_i u^\mu \quad (1.60)$$

where  $n_i$  is the number density of particle  $i$ .

The standard identifications in Statistical Physics:

$$\alpha_i = \mu_i / K_B T \quad (1.61)$$

$$\beta = 1 / K_B T \quad (1.62)$$

where  $\mu_i$  is the chemical potential for species  $i$ ,  $K_B$  the Boltzmann constant and  $T$  the temperature of the fluid, allow us to calculate via eqs. (1.57), (1.59) and (1.60), the functions  $P_i$ ,  $\rho_i$  and  $n_i$ , that is, in particular, the state equation in thermal equilibrium.

The characteristic time  $\tau_i$  for particles of type  $i$  with respect to the process  $i+j+\dots \rightarrow \ell+m+\dots$  is defined by the rate of change of  $n_i$  due to this process:

$$\frac{1}{\tau_i} \equiv - \frac{1}{n_i} \left[ \frac{dn_i}{dt} \right]_{i+j+\dots \rightarrow \ell+m+\dots} \quad (1.63)$$

In the early universe, if  $\tau_i$  is smaller than a characteristic time for the expansion,  $t_u$ , then there is enough time for the process  $i+j+\dots \rightarrow \ell+m+\dots$  to occur, and it thermally couples the  $i$  particles to the cosmic fluid. By contrast, if  $\tau_i \gg t_u$  for every possible process

in which the particles of type  $i$  participate, then this kind of particles are not in thermal equilibrium with the cosmic gas: they are decoupled.

In order to analyse the evolution of the particle populations which constitute the cosmic fluid, it is necessary to compare  $t_u$  with  $\tau_i$  at different temperatures. The function  $\tau_i(T)$  can be evaluated through the Boltzmann equation (1.53), which for R-W metrics implies that:

$$\frac{1}{R^3} \frac{d}{dt} (R^3 n_i) = \int \pi_i C[N_i] \quad (1.64)$$

The function  $t_u(T)$  can be obtained in the framework of a given cosmological model once the state equation is specified. It will be calculated for the standard model.

#### 1.4 THERMAL HISTORY OF THE UNIVERSE

In the framework of the standard cosmological model, the particles capable of being present are the elementary particles of the standard  $SU(3) \times SU(2) \times U(1)$  microphysical model, which are thermally produced. Including new particle types results in a different evolution of the universe, which can be used to test the viability of the hypotheses made about the exotic particle properties (see Chapter 6).

The number density of particle  $i$  can be derived from eqs. (1.57)

and (1.60) above:

$$n_i = \int \pi_i u_\mu p^\mu \left[ \exp(-\mu_i + u_\lambda p^\lambda) / K_B T + 1 \right]^{-1} \quad (1.65)$$

and in general it is a function of the chemical potential and the temperature.

For  $i = \text{photon}$ , except for a range of temperatures in which the photon number is conserved in any process<sup>(8)</sup>, the chemical potential is zero,  $\mu_\gamma = 0$ . As a consequence

$$\mu_i + \mu_{\bar{i}} = 0 \quad (1.66)$$

for any pair of particle-antiparticle in chemical equilibrium, and the chemical potentials will be zero for any pair such that

$$\mu_i = \mu_{\bar{i}} \quad (1.67)$$

or equivalently (see eq. 1.65):

$$n_i = n_{\bar{i}} \quad (1.68)$$

This is the case of nucleons. The baryon number is very low<sup>(9)</sup>

$$L_B = \frac{n_B - n_{\bar{B}}}{n_\gamma} \approx \frac{n_B}{n_\gamma} \approx 0(10^{-10}) \quad (1.69)$$

so that  $\mu_B = 0$ . As for leptons, it is a hypothesis of the standard cosmological model to assume that:

$$L_i = \frac{n_i - n_i^- + n_{\nu_i} - n_{\nu_i}^-}{n_\gamma} \ll 1 \quad (1.70)$$

for  $i = e^-, \mu^-, \tau^-$ , and consequently:

$$\mu_i = \mu_i^- = \mu_{\nu_i} = \mu_{\nu_i}^- = 0 \quad (1.71)$$

If  $\mu_i/K_B T \ll 1$ , then eq. (1.65) gives, in two extreme regimes:

i) For  $K_B T \gg m_i$  (relativistic particles)

$$n_i(\text{boson}) = \frac{1.202}{\pi^2} g_i (K_B T)^3 \quad (1.72)$$

$$n_i(\text{fermion}) = \frac{3}{4} n_i(\text{boson}) \quad (1.73)$$

ii) For  $K_B T \ll m_i$  (non-relativistic particles)

$$n_i = g_i \left[ \frac{m_i K_B T}{2\pi} \right]^{3/2} \exp(-m_i/K_B T) \quad (1.74)$$

which implies that for  $m_i \gg K_B T$ , the particle  $i$  population is exponentially suppressed.

The state equation can be derived from eqs. (1.57), (1.59) and (1.20). We get:

$$\rho_i = \int \pi_i u_\mu u_\nu p^\mu p^\nu [\exp(-\mu_i + u_\lambda p^\lambda)/K_B T + 1]^{-1} \quad (1.75)$$

$$P_i = \frac{1}{3} \int \pi_i (u_\mu u_\nu - g_{\mu\nu}) p^\mu p^\nu [\exp(-\mu_i + u_\lambda p^\lambda)/K_B T + 1]^{-1} \quad (1.76)$$

If  $\mu_i/K_B T \ll 1$ , they lead to:

i) Relativistic particles:

$$\rho_i(\text{boson}) = \frac{\pi^2 g_i}{30} (K_B T)^4 \quad (1.77)$$

$$\rho_i(\text{fermion}) = \frac{7}{8} \rho_i(\text{boson}) \quad (1.78)$$

$$P_i = \frac{1}{3} \rho_i \quad (1.79)$$

ii) Non-relativistic particles:

$$\rho_i = m_i n_i \quad (1.80)$$

$$P_i = n_i K_B T \quad (1.81)$$

The energy conservation equation (1.31) requires that the energy density of a gas of relativistic particles decreases with  $R$  as  $R^{-4}$ , while for non-relativistic particles it varies as  $R^{-3}$ .

The energy density for the relativistic species present at temperature  $T$  can be written as (see eqs. (1.77) and (1.78)):

$$\rho_R(T) = \frac{\pi^2 g_{\text{eff}}(T)}{30} (K_B T)^4 = \frac{g_{\text{eff}}(T)}{2} a T^4 \quad (1.83)$$

where  $a$  is the black-body constant and  $g_{\text{eff}}$  is the effective number of degrees of freedom at temperature  $T$ :

$$g_{\text{eff}}(T) \approx \sum_b g_b \left[ \frac{T_b}{T} \right]^4 + \frac{7}{8} \sum_f g_f \left[ \frac{T_f}{T} \right]^4 \quad (1.84)$$

where a b(f) subscript stands for bosons (fermions) and the sums include all the bosons and fermions present at temperature T, that is, such that  $m_b \lesssim K_B T$  or  $m_f \lesssim K_B T$ . When  $m_i > K_B T$ , the pairs  $i\bar{i}$  annihilate leaving only a trace population. The function  $g_{\text{eff}}(T)$  for the standard model is depicted in figure 1.1<sup>(10)</sup>, where the dominant constituents of the cosmic soup for each temperature range are also shown.

The baryonic contribution to the energy density of the universe exceeds that of relativistic particles at present. In fact, the only relativistic constituents of the cosmic fluid at the present time are photons and neutrinos, so that:

$$\rho_{R0} \approx K_B T_0 n_{\gamma 0} \quad (1.85)$$

while, for baryons at the present time:

$$\rho_{B0} = m_B n_{B0} \quad (1.86)$$

and then:

$$\frac{\rho_{B0}}{\rho_{R0}} \approx \frac{m_B}{K_B T_0} \eta_0 \approx 10^{12} \eta_0 \quad (1.87)$$

for  $T_0 = 2.7 \text{ K}$  (see Chapter 3), where:

$$\eta \equiv \frac{n_B}{n_\gamma} \quad (1.88)$$

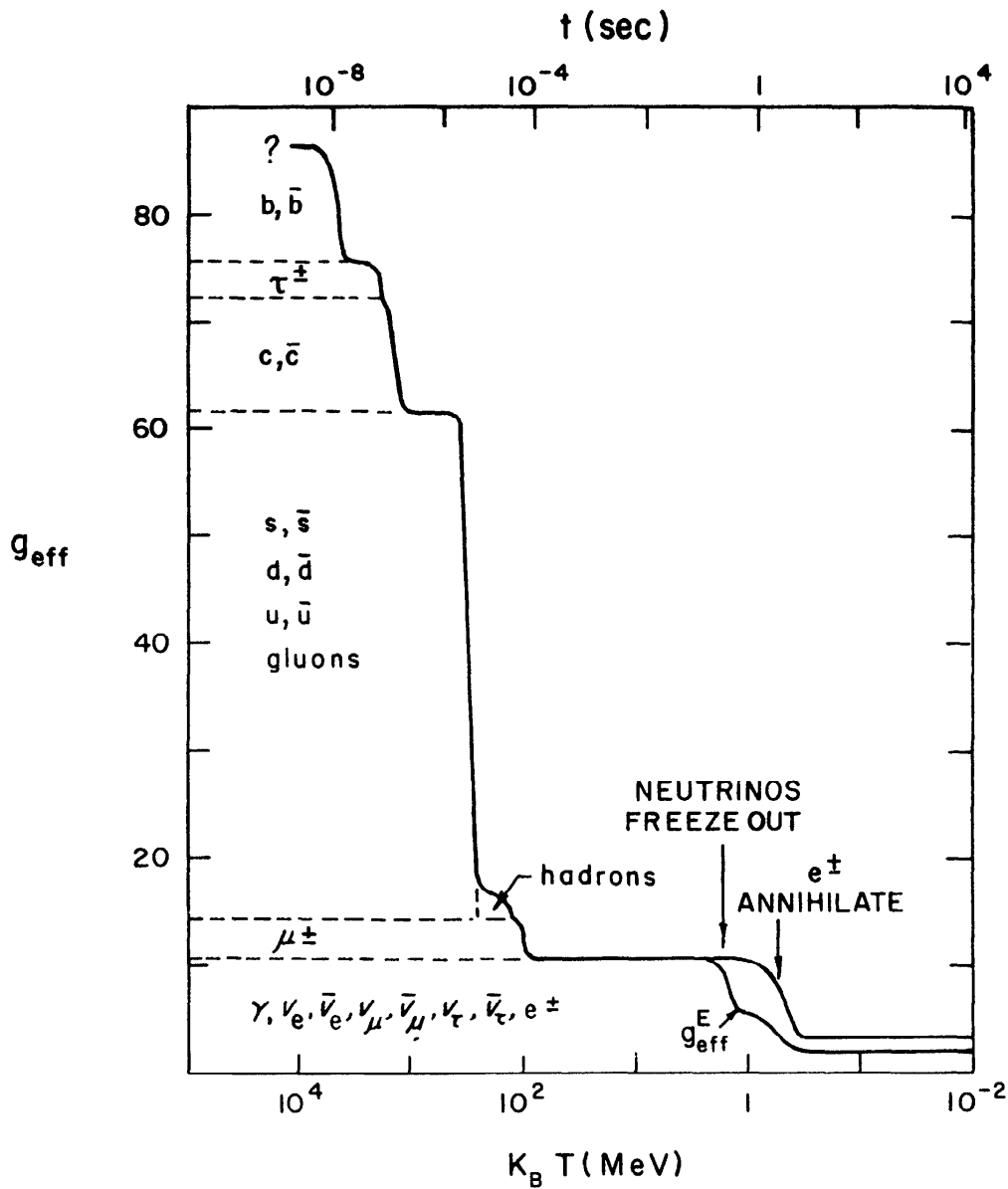


Figure 1.1 The effective number of degrees of freedom  $g_{\text{eff}}$  as a function of the radiation temperature  $T$ . The dominant constituents of the cosmic soup for different temperature ranges are also shown (from Wagoner (10); copyright 1980 by North-Holland Physics Publishing).



is the baryon-to-photon number ratio, a parameter whose present value can be derived from light element abundance observations (see Chapter 4). It is found that<sup>(9)</sup>:

$$3 \times 10^{-10} \leq \eta_0 \leq 10^{-9} \quad (1.89)$$

and consequently:

$$\rho_{B0} \gg \rho_{R0}$$

The baryon-to-photon number ratio  $\eta$  is constant throughout cosmic evolution once the pairs  $e^+e^-$  annihilate (see below). Eq. (1.87) then implies that the universe density could have been dominated by relativistic particles if the universe had once been at temperatures higher than  $T_0$ . In this case, eqs. (1.26), (1.83) and (1.84) allow us to obtain the time-temperature relation for FRW models:

$$t \approx \left[ \frac{45}{16\pi^3 G} \right]^{1/2} \frac{1}{g_{\text{eff}}^{1/2}(T) (K_B T)^2} \quad (1.90)$$

For a density dominated by non-relativistic particles (matter-dominated density), the  $t(T)$  function is

$$t \propto [K_B T]^{-3/2} \quad (1.91)$$

This implies that the universe cools as time passes and the expansion goes on. The universe has indeed been at higher temperatures

in the past, and a temperature  $T_{\text{dom}}$  exists such that:

$$\rho_B(T_{\text{dom}}) = \rho_R(T_{\text{dom}})$$

It is given by (see below):

$$T_{\text{dom}} = 2.40 \times 10^{12} \eta_0 \text{ K} \quad (1.92)$$

and for  $T > T_{\text{dom}}$ , the universe density is dominated by relativistic particles.

The conservation of entropy per comoving volume  $R^3$  of particles in thermal equilibrium,  $S^E$ , as the expansion proceeds is a consequence of the energy conservation for these particles when taken separately<sup>(2)</sup>. At a temperature  $T$  and for relativistic particles,  $S^E$  is given by:

$$S^E = \frac{R^3}{T} \sum_i (\rho_i + P_i) = \frac{2}{3} g_{\text{eff}}^E(T) a T^3 R^3 \quad (1.93)$$

where the sum includes the particles in thermal equilibrium and we have taken into account eqs. (1.79) and (1.83). As a consequence of this conservation law,  $TR$  is constant in the temperature ranges in which  $g_{\text{eff}}^E(T)$  is constant;  $g_{\text{eff}}^E(T)$  is constant except in the neighborhood of a pair annihilation (see figure 1.1). In these cases, eq. (1.93) requires that:

$$\frac{(TR)_b^3}{(TR)_a^3} = \frac{g_{\text{eff},a}^E}{g_{\text{eff},b}^E} \quad (1.94)$$

where the subscript  $b(a)$  stands for the values of the functions before

(after) the pair annihilation. This jump in TR results in a jump in the  $\eta$  parameter given by:

$$\frac{\eta_a}{\eta_b} = \frac{(TR)_b^3}{(TR)_a^3} \quad (1.95)$$

The last annihilated particle pairs are electron-positron pairs, at a temperature  $K_B T \approx 2m_e \approx 1 \text{ MeV}$ . For this annihilation:

$$\frac{(TR)_{<1 \text{ MeV}}^3}{(TR)_{>1 \text{ MeV}}^3} = \frac{11}{4} \quad (1.96)$$

because at  $K_B T \approx 1 \text{ MeV}$ , neutrinos are no longer in thermal equilibrium with the cosmic fluid, and only photons (for  $K_B T \lesssim 1 \text{ MeV}$ ) and  $e^+e^-$  (for  $K_B T \gtrsim 1 \text{ MeV}$ ) enter the calculation of  $g_{\text{eff}}^E$ .

Let us now consider the decoupling temperature for weak interacting particles. For the standard microphysical model, only neutrinos ( $\nu_e, \nu_\mu, \nu_\tau$ ) have such a property. The most important processes in order to keep these particles coupled to the components in thermal equilibrium, are neutral current weak interactions with  $e^\pm$ . Their characteristic time is given approximately by<sup>(10)</sup>:

$$\frac{1}{\tau} \approx \frac{n_e e^4 (K_B T)^2}{\left[ (K_B T)^2 + m_{Z^0}^2 \right]^2} \quad (1.97)$$

where  $m_{Z^0}$  is the neutral weak boson mass and  $e$  the  $e^\pm$  charge. We are thus led to (see eq. (1.90)):

$$\frac{t}{r} \approx \frac{\alpha^2}{g_{\text{eff}}^{1/2}} \frac{M_{\text{Pl}} (K_B T)^3}{[(K_B T)^2 + m_{Z^0}^2]^2} \quad (1.98)$$

The condition  $\frac{t}{r} \gg 1$  holds for

$$\text{few MeV} \approx \left[ \frac{g_{\text{eff}}^{1/2} m_{Z^0}^4}{\alpha^2 M_{\text{Pl}}} \right]^{1/3} \lesssim K_B T \lesssim \frac{\alpha^2}{g_{\text{eff}}^{1/2}} M_{\text{Pl}} \quad (1.99)$$

where  $\alpha$  is the fine structure constant. Electron neutrinos have also charged current interactions and they decouple at a somewhat lower temperature.

For  $K_B T \lesssim \text{few MeV}$ , neutrinos are then decoupled from the thermal component. Their distribution has the same form of thermal equilibrium<sup>(2)</sup>. Their momentum varies according to  $R^{-1}$  and they are not heated by the  $e^\pm$  annihilation, so that their "temperature" verifies:

$$T_\nu R = \text{constant} \quad (1.100)$$

and then eq. (1.94) implies that:

$$\left[ \frac{T}{T_\nu} \right]_{< 1 \text{ MeV}}^3 = \frac{11}{4} \quad (1.101)$$

so that, for  $K_B T \lesssim 1 \text{ MeV}$  the energy density in relativistic particles is given by:

$$\rho_R(T) = a T^4 + \frac{7}{8} N_\nu a T_\nu^4 \quad (1.102)$$

where  $N_\nu$  is the number of families of light neutrinos. This

expression, with  $N_\nu=3$ , has been used to derive  $T_{\text{dom}}$  (eq. (1.92)).

For  $K_B T \lesssim 1 \text{ MeV}$ , the universe is made of photons, neutrinos, nucleons and electrons. Because the electric charge of the universe is zero, the electron number density equals the proton number density. The nucleons bound to form  ${}^4\text{He}$  nuclei at  $K_B T \approx 1 \text{ MeV}$  (see Chapter 4), which constitutes about 25% of the baryonic mass of the universe. At high temperatures, electrons and nuclei are unbound and they form a plasma, but as the universe cools, a temperature  $T_R$  is reached such that the plasma recombines to form neutral atoms. At this moment the thermal contact between matter and radiation is lost and they became decoupled. A detailed analysis of this process can be found in reference (11), where it is shown that the fraction of ionized material sharply decreases from 99.8% at  $T = 5 \times 10^3 \text{ K}$  to 0.98% at  $T = 3 \times 10^3 \text{ K}$ , for  $\rho_B = 1.8 \times 10^{-29} \text{ gr/cm}^3$ , and that recombination has almost ended at  $T = 2 \times 10^3 \text{ K}$ .

## REFERENCES 1

1. C.M. Will, 1981, "Theory and Experimentation in Gravitational Physics" (Cambridge: Cambridge University Press).
2. S. Weinberg, 1972, "Gravitation and Cosmology" (New York: J. Wiley and Sons).
3. J.D. Barrow, M.N.R.A.S. 175 (1976) 359.
4. A. Friedmann, Z. Phys. 10 (1922) 377.
5. A. Sandage, Observatory 88 (1968) 91.
6. J. Audouze, 1980, in "Physical Cosmology", Les Houches Summer School. R. Balian, J. Audouze and D.N. Schramm eds. (Amsterdam: North-Holland).  
E.M.D. Symbalisty and D.N. Schramm, Rep. Prog. Phys. 44 (1981) 293.  
A. Sandage, Ap. J. 252 (1982) 553.
7. J. Ehlers, 1971, in "General Relativity and Cosmology", Proc. of the International School of Physics Enrico Fermi. R.K. Sachs ed. (New-York: Academic Press).
8. A.D. Dolgov and Ya.B. Zeldovich, Rev. Mod. Phys. 53 (1981) 1.
9. J. Yang, M.S. Turner, G. Steigman, D.N. Schramm and K.A. Olive, Ap. J. 281 (1984) 493.
10. R.V. Wagoner, 1980, in "Physical Cosmology", op. cit.
11. P.J.E. Peebles, Ap. J. 153 (1968) 1.

## CHAPTER 2

# DETERMINATION OF THE COSMOLOGICAL PARAMETERS

The standard cosmological model is determined once the present values of the Hubble constant,  $H_0$ , the deceleration parameter,  $q_0$  (or the density parameter  $\Omega_0$ ), the temperature of the cosmic microwave background radiation,  $T_0$ , the baryon-to-photon number ratio,  $\eta_0$ , and the number of light neutrino families,  $N_\nu$ , are specified.

In this Chapter the most important methods used to measure  $H_0$ ,  $q_0$  and  $\Omega_0$  are considered. In forthcoming Chapters, the derivation of the  $T_0$ ,  $\eta_0$  and  $N_\nu$  parameters will be discussed.

## 2.1 THE RED-SHIFT

A set of observations to be explained by any viable cosmological model is the red-shift of the spectral lines of extragalactic objects. When interpreted in terms of Döppler shifts, these observations require that galaxies placed beyond the Virgo cluster (whose distance is 21.6 Mpc<sup>(1)</sup>) move away from the Milky Way with a velocity which is proportional to their distance. Red-shifts of closer objects indicate the existence of a local field of velocities due to the density inhomogeneities at these scales<sup>(2)</sup>.

The red-shift of spectral lines can be explained by the expansion of the universe. In fact, let us consider an electromagnetic wave which is emitted at time  $t_E$  and reaches an observing device later on at time  $t_o$ . This light signal follows a radial geodesic ( $\theta = \text{constant}$ ,  $\phi = \text{constant}$ ) in a universe described by a Robertson-Walker metric (1.3) and (1.4). Assuming that the observing device is placed at the origin of a comoving coordinate system and that the point where emission occurs has a radial coordinate  $r_E$ , we are led to:

$$\int_0^{r_E} \frac{dr}{(1-kr^2)^{1/2}} = \int_{t_E}^{t_o} \frac{dt}{R(t)} \quad (2.1)$$

because  $ds^2 = 0$  for light signals. The same equality holds for a photon emitted later on at time  $t_E + \delta t_E$  and observed at time  $t_o + \delta t_o$ .



$$\int_0^{r_E} \frac{dr}{(1-kr^2)^{1/2}} = \int_{t_E + \delta t_E}^{t_o + \delta t_o} \frac{dt}{R(t)} \quad (2.2)$$

If  $\delta t_E = 1/\nu_E$  is the period of the electromagnetic wave at emission, then  $\delta t_o = 1/\nu_o$  will be its period at observation ( $\nu_E$  and  $\nu_o$  are the respective frequencies). Eqs. (2.1) and (2.2) then imply that:

$$1 + z \equiv \frac{\nu_E}{\nu_o} = \frac{R(t_o)}{R(t_E)} \quad (2.3)$$

The shift  $z$  of the spectral lines is operationally defined by this expression, which gives its value as a function of the cosmic scale factor  $R(t)$  at times  $t_E$  and  $t_o$ . Only red-shifts are observed, so that  $z > 0$  and then necessarily  $R(t_o) > R(t_E)$  and the universe expands.

When the emission and observation points are close together,  $t_o \rightarrow t_E$ ,  $r_E \rightarrow 0$  and  $z \ll 1$ . In this case:

$$1 + z \rightarrow 1 + r_E \dot{R}(t_o) = 1 + v_r \quad (2.4)$$

where  $v_r$  is the recession velocity of the source of electromagnetic waves. The cosmological red-shift can then be interpreted in terms of a Döppler shift. On the other hand, for a higher value of  $z$ , the contribution to the frequency change of the gravitational field of the universe has to be taken into account and the interpretation is not so obvious.

## 2.2 THE DETERMINATION OF THE HUBBLE CONSTANT AND THE DECELERATION PARAMETER

Let us consider an extragalactic object whose absolute and apparent luminosities are  $L$  and  $\ell$ , respectively. By analogy with the definition of luminosity distance for a light source in Euclidean geometry, its luminosity distance is defined by the expression:

$$d_L \equiv \left[ \frac{L}{4\pi\ell} \right]^{1/2} = 10^{-5 + \frac{m-M}{5}} \text{ Mpc} \quad (2.5)$$

where  $m$  is the apparent magnitude of the object, defined by:

$$m = -2.5 \log \ell + C \quad (2.6)$$

with  $C$  a constant which fixes the zero point of the magnitude scale.  $M$  is the absolute magnitude of the light source, that is, its apparent magnitude when placed at 10 pc. The difference  $m-M$  does not depend on  $C$  and it defines  $d_L$ ; this is called "the distance modulus".

It can be shown<sup>(3)</sup> that  $d_L$  is related to the radial coordinate of the source by:

$$d_L = r_E \frac{R^2(t_o)}{R(t_E)} \quad (2.7)$$

for any  $R$ - $W$  type metric. For FRW cosmological models whose energy density is at present matter-dominated,  $r_E$  can be expressed in terms of the source red-shift and the cosmological parameters  $H_0$  and  $q_0$ :

$$r_E = \frac{zq_0 + (q_0 - 1)[(1 + 2q_0 z)^{\frac{1}{2}} - 1]}{H_0 R_0 q_0^2 (1 + z)} \quad (2.8)$$

and according to eqs. (2.5) and (2.7) we are then led to:

$$m - M = 25 - 5 \log H_0 (\text{km s}^{-1} \text{Mpc}^{-1}) + 5 \log \left\{ \frac{zq_0 + (q_0 - 1)[(1 + 2q_0 z)^{\frac{1}{2}} - 1]}{q_0^2} \right\} \quad (2.9)$$

If the time elapsed since emission of the light signal up to its observation is short compared to the Hubble time  $H_0^{-1}$  (or, equivalently,  $z \ll 1$ ), a series expansion of eq. (2.9) allows us to write:

$$m - M = 25 - 5 \log H_0 (\text{km s}^{-1} \text{Mpc}^{-1}) + 5 \log cz (\text{km s}^{-1}) + 1.086 (1 - q_0) z + \dots \quad (2.10)$$

which holds for any R-W type metric in this approximation. This expression, when plotted for a particular group of astronomical objects of fixed absolute magnitude (standard candles) constitutes what is known as the Hubble diagram. It predicts a linear dependence of the apparent magnitude of a set of standard candles as a function of their red-shift for objects with low value of  $z$ . For higher values of  $z$ , the shape of the curve depends on  $q_0$ , and then could serve, in principle, as a method of deriving  $q_0$ .

#### DETERMINATION OF $H_0$

In order to derive the Hubble constant through the expression (2.9), we need to know the red-shift and the apparent and absolute

magnitudes of a single object placed beyond the Virgo cluster (or even further away if large scale streaming motions are confirmed, see Section 5.2) and with  $z \lesssim 0.1$ . The determination of  $z$  and  $m$  does not raise any major problem. The difficulties lie in the absolute magnitude measurement, which is equivalent to the determination of the distance at which the object is placed. The measurement of extragalactic distances is usually done by means of standard candles, that is, a class of astronomical objects whose absolute magnitude is uniform and of known value. Different standard candles are used for increasing distances, and the determination of their absolute magnitude is made in the step previous to that in which the standard candle in question is used as a distance indicator. An introduction to the determination of the extragalactic distance scale can be found in reference (3).

Brightest cluster galaxies have been used as standard candles for the most distant objects. A detailed discussion of the method followed by G.A. Tammann and A. Sandage's group is made in reference (4). This group found that:

$$H_0 = 50 \pm 10 \text{ km s}^{-1} \text{ Mpc}^{-1} \quad (2.11)$$

while G. de Vaucouleurs' group give<sup>(5)</sup>

$$H_0 = 100 \pm 10 \text{ km s}^{-1} \text{ Mpc}^{-1} \quad (2.12)$$

Supernovae have been estimated to have an uniform maximum absolute luminosity with small dispersion about the mean, and they can consequently be used as standard candles. Type I supernovae are considered to yield at present the most reliable determination of the

large scale  $H_0$  by Tammann and Sandage. They find that<sup>(6)</sup>

$$H_0 = 50 \pm 7 \text{ km s}^{-1} \text{ Mpc}^{-1} \quad (2.13)$$

while G. de Vaucouleurs' group obtain by this method the following value for the Hubble ratio<sup>(7)</sup>:

$$H_c = 99 \pm 8 \text{ km s}^{-1} \text{ Mpc}^{-1} \quad (2.14)$$

Another largely utilized distance indicator is the global HI line width profile, which has been found to be correlated to the galaxy luminosity by Tully and Fisher<sup>(8)</sup>. To avoid the uncertainties in the absorption corrections, Aaronson et al. have proposed using infrared magnitudes. They derive a "best guess" value for the Hubble constant of<sup>(9)</sup>

$$H_0 = 90 \text{ km s}^{-1} \text{ Mpc}^{-1} \quad (2.15)$$

The differences among different authors are mainly due to the calibration methods employed for the local distance scale and to the way in which the galactic extinction correction is carried out. They are delicate technical problems and it is difficult to decide which one is the correct value. The Hubble constant is usually parametrized in the way:

$$H_0 = 100h \text{ km s}^{-1} \text{ Mpc}^{-1} \quad (2.16)$$

and  $h$  is taken to be

$$\frac{1}{2} \leq h \leq 1 \quad (2.17)$$

The calibration methods are expected to be improved with the help of the Space Telescope<sup>(9)</sup>.

Very-long-baseline radio interferometry techniques have been recently applied to measure the angular size of the shell of debris ejected by the recent supernova SN1979c in the galaxy M100 in the Virgo cluster, which exploded in 1979 and which is expanding with velocity  $v_r = 1.2 \times 10^4 \text{ km s}^{-1}$  (known from optical observations). This gives the real size of the photosphere. The real size of the radiosphere can be known by means of a model relating the photosphere and the radiosphere, and making a comparison with its angular size gives the distance to the Virgo cluster and  $H_0$ . It has been found that<sup>(10)</sup>:

$$H_0^{(\text{local})} = 65_{-25}^{+35} \text{ km s}^{-1} \text{ Mpc}^{-1} \quad (2.18)$$

Errors are mainly due to the fact that the derivation is model dependent.

It is hoped that in the future it will be possible to measure the angular sizes of the photosphere ejected by supernovae explosions by means of the Space Telescope<sup>(11)</sup>. This will lower the errors in the determination of  $H_0$  from observations of the expanding shells resulting from supernovae explosions.

For recent reviews on the cosmic distance scale determinations, see reference (12).

## DETERMINATION OF $q_0$

The present deceleration parameter  $q_0$  and density parameter  $\Omega_0$  are related by ( $P_0 \approx 0$ )

$$\Omega_0 = 2q_0 + \frac{2}{3} \frac{\Lambda}{H_0^2} \quad (2.19)$$

If  $\Lambda = 0$ , determining  $q_0$  gives  $\Omega_0$  and conversely. An independent derivation of  $q_0$  and  $\Omega_0$  gives  $\Lambda$ .

It is not possible to derive  $q_0$  by means of the Hubble diagram for some kinds of standard candles due to their evolution. In fact, let us assume that the intrinsic luminosity of an object in a given band depends on time,  $L = L(t)$ . If this function is developed as a series of  $(t_0 - t_E)$  and the reasoning pattern leading to eq. (2.10) is repeated, we will obtain an expression formally identical to eq. (2.10), but with  $q_{0,eff}$  instead of  $q_0$ , where:

$$q_{0,eff} = q_0 - \frac{\dot{L}(t_0)}{L(t_0)H_0} = q_0 + \Delta q_0 \quad (2.20)$$

This means that the Hubble diagram gives information about  $q_{0,eff}$ , which differs from the true  $q_0$  in the evolutionary term  $\Delta q_0$ .

B.M. Tinsley and J.E. Gunn<sup>(13)</sup> have evaluated the correcting term  $\Delta q_0$  for the optical luminosity of galaxies, by modelling the effects of stellar evolution and of the supposed cannibalism of the brightest cluster members. The resulting correction depends on the details of the model and on the cosmological model, but is always of the same order as  $q_{0,eff}$  as given by the Hubble diagram for brightest cluster galaxies (best fit:  $q_{0,eff} = 1.6$ ). Later galaxy evolution

models by Bruzual<sup>(14)</sup> confirmed that the Hubble diagram for galaxies in the V-band is useless for determining  $q_0$ . However, infrared K-band Hubble diagrams are more sensitive to cosmological parameters than to evolutionary effects, and they could possibly be used to derive  $q_0$ <sup>(15)</sup> (see figure 2.1).

Considering other kind of extragalactic objects as standard candles does not improve the situation, except for supernovae. The value of their maximum absolute magnitudes is assumed to be independent of the cosmological epoch, because they are due to local physical conditions that are the same in

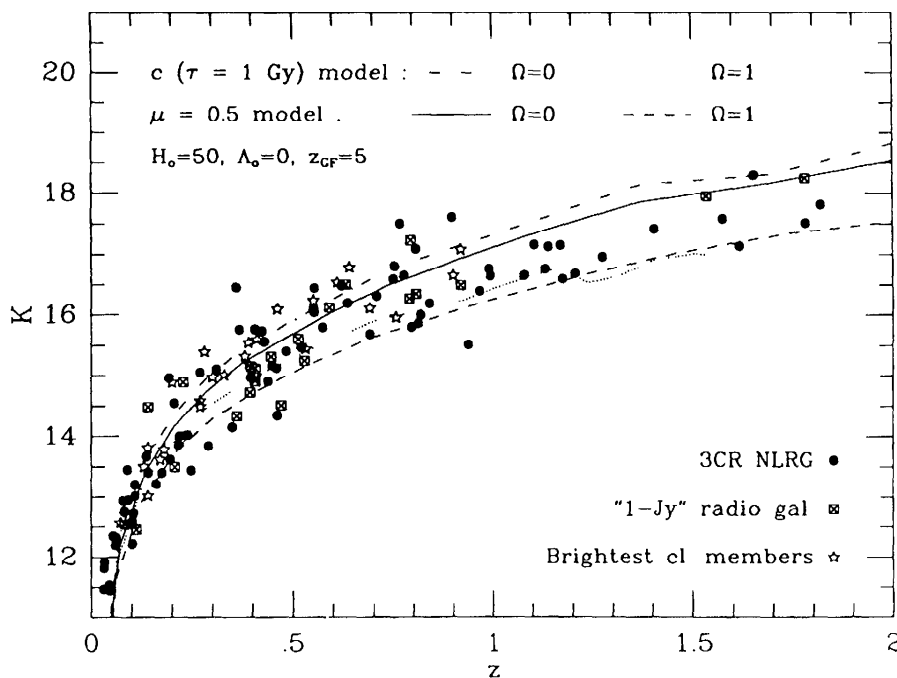


**Figure 2.1** The currently available K-band photometry for distant galaxies. Superposed are the galaxy evolution models by Bruzual, characterized either by a single 1-Gyr burst of star formation (c-models), or an exponentially decreasing star formation rate ( $\mu$ -models) and by deceleration parameters of  $q_0 = 0$  and  $q_0 = \frac{1}{2}$  (from Spinrad and Djorgovski (15); copyright 1987 by the IAU).



any explosion. Consequently, there are no evolutionary corrections for the Hubble diagram for supernovae. The problem now is that in order to measure  $q_0$ , objects at high red-shift ( $z \gtrsim 0.5$ ) are needed, and at these distances supernovae are too weak to be detected from terrestrial telescopes: this will only be possible by means of the Space Telescope<sup>(16)</sup>. With this telescope it is expected that  $q_0$  could be determined with an error lower than 0.15 from observations of supernovae in rich galaxy clusters.

### 2.3 DETERMINATION OF THE DENSITY PARAMETER

The determination of the mean energy density in the form of gravitationally bound mass is carried out by means of dynamical methods, which are unable to distinguish between nucleons and another kind of gravitating material (for example, massive neutrinos, axions, photinos...).

At the scale of galaxies and galaxy clusters, these methods measure the mass-to-light ratios,  $M/L$ , and the mean density is derived by means of the expression:

$$\rho = \frac{M}{L} \varpi \quad (2.21)$$

where  $\varpi$  is the average luminosity density of the night sky. The density parameter  $\Omega$  on a given scale can also be determined:

$$\Omega = \frac{M/L}{(M/L)_c} \quad (2.22)$$

where the critical mass-to-luminosity ratio is defined by:

$$(M/L)_c = \rho_c / \mathcal{L} \quad (2.23)$$

Here  $\rho_c$  is the critical density for universe closure.

Two kinds of uncertainties arise in this method. The first of them is the  $\mathcal{L}$  value<sup>(17)</sup>. Kirshner, Oemler and Schechter give

$$\mathcal{L} = (1.9 \pm 0.28) \times 10^8 h L_{\odot} \text{ Mpc}^{-3} \quad (2.24)$$

with  $L_{\odot}$  the solar luminosity,  $L_{\odot} = 3.9 \times 10^{33} \text{ erg s}^{-1}$ . Davis, Geller and Huchra find:

$$\mathcal{L} = 1.2 \times 10^8 h L_{\odot} \text{ Mpc}^{-3} \quad (2.25)$$

and Yahil, Sandage and Tammann

$$\mathcal{L} = 1.56 \times 10^8 h L_{\odot} \text{ Mpc}^{-3} \quad (2.26)$$

That is, there exists an uncertainty of roughly a factor of two in the  $\mathcal{L}$  value.

The second problem lies in the M/L determination. A detailed review on the different methods to derive the mass-to-luminosity ratio in spiral and elliptical galaxies can be found in reference (18). Here only the major results will be quoted.

i) A direct determination of M/L can only be achieved in the solar neighborhood. It has been found that<sup>(19)</sup>

$$\frac{M}{L} = (2 \pm 1) \frac{M_{\odot}}{L_{\odot}} \quad (2.27)$$

where  $M_{\odot}$  is the solar mass,  $M_{\odot} = 2 \times 10^{33}$  g. Taking  $\varpi = 2 \times 10^8$  h  $L_{\odot}$   $\text{Mpc}^{-3}$ , this leads to:

$$\Omega_0 = (0.0016 \pm 0.0008) h^{-1} \quad (2.28)$$

It has been pointed out<sup>(20)</sup> that about 50% of the mass in the solar vicinity could be in the form of unobserved material.

ii) The observation of the 21 cm line in galactic HI regions shows that the rotation curve of the Milky Way is flat beyond the Sun up to several kpc. (The rotation curve is the representation of the velocity of rotation of the HI regions as a function of their distance to the galactic center). These observations, together with the analysis of radial velocities of globular clusters and nearby dwarf spheroidal galaxies<sup>(21)</sup>, permit us to know the mass distribution inside a radius R. This distribution implies the existence of a dark halo, which goes further away from the luminous component, giving  $M/L \lesssim (70 \pm 20) M_{\odot}/L_{\odot}$ .

### iii) Spiral galaxies

Rotation curves from the 21 cm line observations in HI regions are known for spiral galaxies beyond the Holmberg radius  $R_H$  (radius of the isophote of  $m_{pg} = 26^m \cdot 5 \text{ arc sec}^{-2}$ ). They show that, in contrast with standard Newtonian mechanics predictions, the tangential velocities do not decrease as  $v(R) \propto R^{-1/2}$  for large values of R, but

they tend to a constant  $v_c$  ( $\sim 150-300 \text{ km s}^{-1}$  for bright spirals). Figure 2.2<sup>(22)</sup> shows some of these rotation curves. Newtonian mechanics allows us to calculate the mass inside a radius  $R$ :

$$M(<R) = \frac{R v_c^2}{G} \quad (2.29)$$

which requires that:

$$\rho(R) \propto R^{-2} \quad (2.30)$$

The optical and infrared density of stellar luminosity varies as<sup>(23)</sup>

$$j(R) \propto R^{-3} \quad (2.31)$$

which when compared with eq. (2.30) suggests that the gravitating mass density has not the same distribution as the observable stars. It is then necessary to postulate a dark component at large values of  $R$ , which is known as the halo (see, however, Lafon<sup>(24)</sup> for a different opinion, and Milgrom<sup>(25)</sup> for a modification of the gravitation laws at large scale, which implies flat rotation curves).

Analysis of rotation curves shows that in the central regions of spiral galaxies:

$$\frac{M(<R_H)}{L(<R_H)} \approx (4-20) h \frac{M_\odot}{L_\odot} \quad (2.32)$$

which does not greatly differ from the solar vicinity value (2.27) if

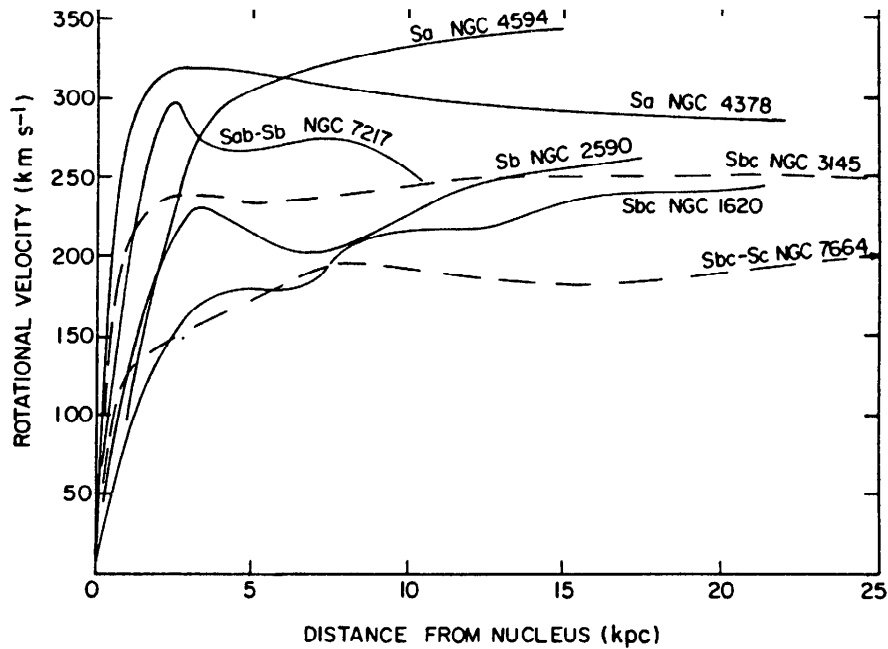


**Figure 2.2** Rotational velocities for seven galaxies, as a function of distance from nucleus. Curves have been smoothed to remove velocity undulations across arms and small differences between major-axis velocities on each side of nucleus (from Rubin, Ford and Thonnard (22); published by the University of Chicago Press; copyright 1978 by the AAS).

$h = 1/2$ . In contrast, statistics of binaries spiral-spiral and the rotation curves at large  $R$ , point to <sup>(22,26)</sup>

$$\frac{M(<100 \text{ kpc})}{L(<100 \text{ kpc})} \approx (60 \pm 20) h \frac{M_{\odot}}{L_{\odot}} \quad (2.33)$$

$$\Omega_0 \approx 0.05 \pm 0.016 \quad (2.34)$$

that is, different methods confirm the presence of a dark component in spiral galaxies on scales  $> R_H$ .

#### iv) Elliptical galaxies

Traditionally, the mass of this kind of galaxies is derived from the virial theorem. This requires knowing some parameters such as  $\langle v^2 \rangle$ , which is not easy to determine. For the central parts of the galaxies, it is found that:

$$\frac{M}{L} \approx (10 - 20) h \frac{M_{\odot}}{L_{\odot}} \quad (2.35)$$

In some cases, elliptical galaxies are surrounded by an X emitting plasma, and then  $M(\langle R \rangle)$  can be derived from the observed density profiles of the X emission (and from the assumption that the plasma is in hydrostatic equilibrium)<sup>(27)</sup>. Another method is the statistical analysis of binaries. The mass-to-light ratios obtained in both cases are similar to those found for the outer regions of spiral galaxies (2.33), so that ellipticals may also have dark halos.

The existence of dark matter in galaxies does not exclude, in principle, that it may be baryonic. This problem has been analysed by Hegyi and Olive<sup>(28)</sup>, who concluded that the only possibility for a baryon dominated halo is that it is formed by black holes which are either primordial or extremely efficient in accreting material. Low mass Jupiter-like objects with masses  $< 0.08 M_{\odot}$  are difficult to exclude, unless the initial mass function (IMF)

$$\phi(m) = A m^{-x} \quad (2.36)$$

(which gives the stellar mass distribution at star formation and is constrained from stellar data in the solar vicinity<sup>(29)</sup>), could be

safely extrapolated toward the low mass region. Bimodal IMF models<sup>(30)</sup> which predict a higher star formation rate for massive stars in the past, and models where the IMF has a metallicity dependent slope,  $x^{(31)}$ , might reinforce the possibility of black hole dominated galactic haloes.

v) Galaxy clusters

High mass-to-light ratios are obtained for relaxed galaxy clusters when they are modelled by means of monomassive isothermal spheres<sup>(32)</sup>

$$\frac{M}{L} \approx (300-600) h \frac{M_{\odot}}{L_{\odot}} \quad (2.37)$$

However, when the model is refined, then lower M/L values can be found. For example all available data of the Coma cluster can be fitted together by means of models which lead to M/L values of<sup>(33)</sup>

$$\frac{M}{L} \approx (150 \pm 40) h \frac{M_{\odot}}{L_{\odot}} \quad (2.38)$$

The density parameter at scale of galaxy clusters has a value of:

$$\Omega_0 \approx 0.12 - 0.5 \quad (2.39)$$

lower than the critical value  $\Omega = 1$ .

vi) The cosmic virial theorem<sup>(34,35)</sup> connects the galaxy peculiar velocities due to inhomogeneities of the density field on scales  $r$  and these inhomogeneities:

$$\langle v^2(r) \rangle \approx \frac{3}{2} \Omega_0 H_0^2 J_2(r) \quad (2.40)$$

where

$$J_2(r) = \int_0^r s \xi(s) ds \quad (2.41)$$

and  $\xi(s)$  is the galaxy two-point correlation function, derivable from galaxy catalogues (see Chapter 5) and  $\langle v^2(r) \rangle$  is the velocity dispersion for galaxies separated by a distance  $r$ , which can be obtained from complete red-shift samples. The following values of  $\Omega_0$  have been obtained by different authors:

$$\Omega_0 = 0.25 - 0.30 \quad (36) \quad (2.42)$$

$$\Omega_0 = 0.2 e^{\pm 0.4} \quad (37) \quad (2.43)$$

on scales of some tens of Mpc.

Similar values are obtained from the analysis of the Virgocentric flow:

$$\Omega_0 = 0.4 \pm 0.1 \quad (38) \quad (2.44)$$

$$\Omega_0 = 0.35 \pm 0.15 \quad (39) \quad (2.45)$$

These methods would not have detected a density component homogeneous on the scales in consideration.

vii) IRAS galaxies have been used to determine the dipole



component of the local ( $\lesssim 200 h^{-1}$  Mpc) gravitational field<sup>(40)</sup>. It has been found to reasonably agree with the cosmic microwave dipole anisotropy. If this is the case, then the density structure of these galaxies can be used to derive  $\Omega_0$ . In fact, the peculiar velocity  $\vec{u}$  of the Local Group is related to  $\Omega_0$  by the expression<sup>(34)</sup>

$$\vec{u} = \frac{1}{4\pi} \Omega_0^{0.6} H_0 \int \frac{D(\vec{r}) \vec{r}}{r^3} d^3r \quad (2.46)$$

where  $D(\vec{r})$  is the local relative density function of the mass distribution causing the peculiar velocity, which can be derived from galaxy counts. It is found that:

$$\Omega_0 = 1 \pm 0.2 \quad (2.47)$$

The quoted errors are only statistical, and may remarkably underestimate the total error. The disagreement between this value and those deduced from the cosmic virial theorem and the Virgo-centric infall could be real, however.

Another indication of an  $\Omega_0$  of about unity, comes from its measurement using deep galaxy counts (median red-shift  $z = 0.5$ , scales  $\sim 1000 h^{-1}$  Mpc). They lead to<sup>(41)</sup>

$$\Omega_0 = 0.9_{-0.5}^{+0.7} \quad (2.48)$$

Here also the error evaluation is uncertain.

From this short review on the  $\Omega_0$  determinations on different scales, we conclude that  $\Omega_0$  increases with scale, and even if still controversial, some indications exist that it could be as large as

$\Omega_0 = 1$  on scales of  $\gtrsim 100 h^{-1}$  Mpc, in agreement with the inflationary scenario predictions (see Chapter 9). This fact indicates the existence of dark matter and the subsequent question to answer concerns the microphysical properties of such a material. The most stringent constraints against dark matter being baryons is provided by primordial nucleosynthesis in standard cosmological frameworks. In fact, when calculated outputs are compared with light element abundance observations, agreement is only reached for a limited range of the baryon-to-photon ratio, namely<sup>(42)</sup>

$$\eta_{\min} \equiv 3 \times 10^{-10} \leq \eta_0 \leq 10^{-9} \equiv \eta_{\max} \quad (2.49)$$

which results in an upper limit for the baryonic contribution to  $\Omega_0$

$$\Omega_{B_0} \leq 3.53 \times 10^{-2} h^{-2} \left[ \frac{T_0}{2.7\text{K}} \right]^3 \quad (2.50)$$

that is, the universe cannot be closed by baryons, and even if  $\Omega_0 \approx 0.1 - 0.3$ , non-baryonic dark matter could possibly be necessary to explain the astronomical data. Some ways-out to the limit (2.49) will be addressed in Chapter 6.

## REFERENCES 2

1. A. Sandage and G.A. Tammann, 1982, in "Astrophysical Cosmology: Proceedings of the Study Week on Cosmology and Fundamental Physics", H.A. Brück, G.V. Coyne and M.S. Longair eds. (Rome: Specola Vaticane).  
A. Sandage and G.A. Tammann, Nature 307 (1984) 326.
2. A. Yahil, A. Sandage and G.A. Tammann, 1980, in "Physical Cosmology", Les Houches Summer School, R. Balian, J. Audouze and D.N. Schramm eds. (Amsterdam: North-Holland).  
G.A. Tammann and A. Sandage, Ap. J. 294 (1985) 81.  
M. Aaronson, J. Huchra, J. Mould, P.L. Schechter and R.B. Tully, Ap. J. 258 (1982) 64.
3. S. Weinberg, 1972, "Gravitation and Cosmology" (New York: J. Wiley & Sons).
4. G.A. Tammann, A. Sandage and A. Yahil, 1980, in "Physical Cosmology", op. cit.
5. G. de Vaucouleurs, 1982, "The Cosmic Distance Scale and the Hubble Constant" (Canberra: Australian Nat. Univ.).  
G. de Vaucouleurs, Ap. J. 233 (1979) 433.
6. A. Sandage and G.A. Tammann, 1985, "Supernovae as Distance Indicators" (Berlin: Springer-Verlag).  
G.A. Tammann and A. Sandage, Highlights of Astronomy, 6 (1983) 301.
7. G. de Vaucouleurs and H.G. Corwin Jr, Ap. J. 297 (1985) 23.
8. R.B. Tully and J.R. Fisher, Astron. Astrophys. 54 (1977) 661.
9. M. Aaronson and J. Mould, Ap. J. 303 (1987) 1.
10. N. Bartel, A.E.E. Rogers, I.I. Shapiro, M.V. Gorenstein, C.R. Gwinn, J.M. Marcaide and K.W. Weiler, Nature 318 (1985) 25.
11. R.V. Wagoner, Ap. J. Lett. 250 (1981) L65.
12. P.W. Hodge, Ann. Rev. Astron. Astrophys. 19 (1981) 357.  
M. Rowan-Robinson, 1985, "The Cosmological Distance Ladder" (New York: Freeman).
13. B.M. Tinsley, 1977, in "Décalage vers le Rouge et Expansion de l'Univers - L'Evolution des Galaxies et ses Implications Cosmologiques" C. Balkowski and B.E. Westerlund eds. (Paris: CNRS).  
J.E. Gunn, 1978, in "Observational Cosmology" A. Maeder, L. Martinet and G.A. Tammann eds. (Sauverny: Geneva Observatory).
14. G. Bruzual, Ap. J. 273 (1983) 105; 1986, in "Spectral Evolution of Galaxies", C. Chiosi and A. Renzini eds. (Dordrecht: Reidel).
15. H. Spinrad and S. Djorgovski, 1987, in IAU Symposium No. 124 "Observational Cosmology", A. Hewitt, G. Burbidge and Li Zhi Fang eds. (Dordrecht: Reidel).
16. V. Trimble, 1983, in IAU Symposium No. 104 "Early Evolution of the Universe and its Present Structure", G.O. Abell and G. Chincarini eds. (Dordrecht: Reidel).
17. R.P. Kirshner, A. Oemler Jr. and P.L. Schechter, A. J. 84 (1979) 951.  
M. Davis, M.J. Geller and J. Huchra, Ap. J. 221 (1978) 1.  
A. Yahil, A. Sandage and G.A. Tammann, Ap. J. 242 (1980) 448.
18. S.M. Faber and J.S. Gallagher, Ann. Rev. Astron. Astrophys. 17 (1979) 135.
19. M. Joeveer and J. Einasto, Tartu Astron. Obs. Teated 54 (1976) 77.  
G.A. Starikova, Astron. Zh. 37 (1960) 476.
20. J.N. Bahcall, Ap. J. 287 (1984) 926.

21. M.P. Fitzgerald, P.D. Jackson, A.F.J. Moffat, 1978, in IAU Symposium No. 77 "Structure and Properties of Nearby Galaxies", E.M. Berkhuijsen and R. Wielebinski eds. (Dordrecht: Reidel).  
F.D.A. Hartwick and W.L.W. Sargent Ap. J. 221 (1978) 512.
22. V.C. Rubin, W.K. Ford Jr. and N. Thonnard, Ap. J. Lett. 225 (1978) L107.
23. G. de Vaucouleurs and J.L. Nieto, Ap. J. 220 (1978) 449.  
S.P. Boughn and P.R. Saulson, Ap. J. Lett. 265 (1983) L55.
24. J.P.J. Lafon, Astron. Astrophys. 46 (1976) 461.
25. M. Milgrom, Ap. J. 270 (1983) 365.
26. E.L. Turner, Ap. J. 208 (1976) 20 and 304.  
S. Peterson, 1978, Ph.D. thesis, Cornell University, Ithaca, NY.
27. D. Fabricant and P. Gorenstein, Ap. J. 267 (1983) 535.  
W. Forman, C. Jones and W. Tucker, Ap. J. 293 (1985) 102.
28. D.J. Hegyi and K.A. Olive, Phys. Lett. 126B (1983) 28.  
D.J. Hegyi and K.A. Olive, Ap. J. 303 (1986) 56.
29. B.M. Tinsley and J.E. Gunn, Ap. J. 203 (1976) 52.  
G.E. Miller and J.M. Scalo, Ap. J. Suppl. 41 (1979) 513.
30. R.B. Larson, M.N.R.A.S. 218 (1986) 409.
31. R. Terlevich, 1986, in "Star Forming Dwarf Galaxies and Related Objects", D. Kunth ed. (Gift-sur-Yvette: Frontieres)
32. P.J.E. Peebles, A.J. 80 (1979) 730.  
P.J.E. Peebles, 1980, in "Physical Cosmology", op. cit.
33. G. des Forêts, R. Domínguez-Tenreiro, D. Gerbal, G. Mathez, A. Mazure and E. Salvador-Solé, Ap. J. 280 (1984) 15.  
L.L. Cowie, M. Henriksen and R. Mushotzky, Ap. J. 317 (1987) 593.
34. P.J.E. Peebles, 1980, in "Large Scale Structure of the Universe" (Princeton: Princeton University Press).
35. B.J.T. Jones and E. Martínez, 1985, in "Observational and Theoretical Aspects of Relativistic Astrophysics and Cosmology" U.I.M.P. Santander. J.L. Sanz and L.J. Goicoechea eds. (Singapore: World Scientific).
36. P.J.E. Peebles, Ap. J. Lett. 205 (1976) L109.
37. M. Davis and P.J.E. Peebles, Ap. J. 267 (1983) 465.
38. M. Davis, J. Tonry, J. Huchra and D.W. Latham, Ap. J. Lett. 238 (1980) L113.
39. M. Davis and P.J.E. Peebles, Ann. Rev. Astron. Astrophys. 21 (1983) 109.
40. A. Yahil, D. Walker and M. Rowan-Robinson, Ap. J. Lett. 301 (1986) L1.
41. E.D. Loh and E.J. Spillar, Ap. J. Lett. 307 (1986) L1.
42. J. Yang, M.S. Turner, G. Steigman, D.N. Schramm and K.A. Olive, Ap. J. 281 (1984) 493.

## CHAPTER 3

### THE COSMIC MICROWAVE BACKGROUND

As explained in Chapter 1, the dynamical evolution of the universe is characterized by an expansion which results in a decrease of the temperature of the cosmic constituents. Below  $T \approx 1$  MeV, the cosmic gas consists of photons and electron and baryon traces which are in thermal equilibrium with the radiation until the temperature reaches a value  $T_R \approx 4000$  K, and decoupled neutrinos at "temperature"  $T_\nu$ . When  $T < T_R$ , electrons and nuclei recombine forming neutral atoms. Then matter becomes transparent to radiation and the thermal contact between these components is lost.

One of the clearest pieces of evidence for the big-bang model was the discovery of the cosmic microwave background (CMB) by Penzias and Wilson in 1965<sup>(1)</sup>. Its existence had been predicted by Gamow and co-workers in 1946<sup>(2)</sup>, and later on by Dicke, Peebles, Roll and Wilkinson in 1965<sup>(3)</sup>. Subsequent measurements stated that it has a

blackbody spectrum corresponding to a temperature of  $2.75 \text{ K}^{(4)}$ , without any significant distortion.

There exists agreement on the origins of the CMB: the photon gas which dominated the energy density of the universe at high temperatures, even if extremely red-shifted, is still present nowadays. Its Planckian spectrum and isotropy on any scale can be satisfactorily interpreted in the framework of any cosmological model based on the Cosmological Principle and such that: i) the energy-momentum tensor is conserved, ii) the radiation temperature has once been higher than  $T_R$  (to ensure that radiation has once been in thermal equilibrium with matter), and iii) the photon entropy per baryon is much higher than unity.

### 3.1 THE SPECTRUM OF THE COSMIC MICROWAVE BACKGROUND

#### 3.1.1 STANDARD COSMOLOGICAL MODEL PREDICTIONS

We will now analyse which kind of CMB spectrum can be expected to be measured today for the radiation field filling a universe which evolves as described in Chapter 1. Here we are only interested in the constituents of the cosmic gas which are in thermal equilibrium with the radiation when  $T > T_R$ , that is photons, electrons and nuclei: they constitute a plasma. The spectral distribution of the photon energy results from the consideration of the different absorption and emission processes occurring in the cosmic plasma<sup>(5,6)</sup>.

Let  $n_\gamma(\nu_0, t) d\nu_0$  be the number density at time  $t$  of photons which at the present or observing time have a frequency in the interval  $[\nu_0, \nu_0 + d\nu_0]$ . If no absorption or emission process takes place in the medium, then the photon number density in the covolume  $R^3$  must be conserved and:

$$n_\gamma(\nu_0, t) R^3(t) d\nu_0 \equiv N(\nu_0, t) d\nu_0 = \text{constant} \quad (3.1)$$

Absorption and stimulated emission processes cause a modification in  $N(\nu_0, t) d\nu_0$  in the time between  $t$  and  $t+dt$  given by

$$[E(\nu(t), t) - A(\nu(t), t)] N(\nu_0, t) dt d\nu_0$$

where

$$\nu(t) = \nu_0 \frac{R_0}{R(t)} \quad (3.2)$$

is the frequency at time  $t$  of photons of frequency  $\nu_0$  at observation, and  $R_0 = R(t_0)$ .  $E(\nu, t)$  and  $A(\nu, t)$  stand for the stimulated emission and absorption rates at time  $t$  for photons of frequency  $\nu$ , per unit proper volume. Spontaneous emission in the medium adds

$$E'(\nu(t), t) R^3(t) d\nu dt$$

photons to the present number in the same time and energy ranges ( $E'(\nu, t)$  is the spontaneous emission rate at time  $t$  for photons of frequency  $\nu$ , per unit proper volume). The variation rate for the number of photons which have frequency  $\nu_0$  at  $t_0$ , is described by the differential equation

$$\frac{d}{dt} N(\nu_0, t) = [E(\nu, t) - A(\nu, t)] N(\nu_0, t) + E'(\nu, t) R^2 R_0 \quad (3.3)$$

where the time dependence of  $\nu$  and  $R$  has been dropped.

Scattering processes occurring in the plasma should also be taken into account. The most important of these is Thomson scattering, which, due to the fact that the photon energy and  $K_B T$  are much lower than the electron mass, does not change the photon frequency, only its direction. However this has no effect in an isotropic medium such as the one under consideration. The other scattering processes will be assumed to be negligible when compared with absorption.

If the medium is in thermal equilibrium, by using the relations between  $A$  and  $E$ , and between  $E$  and  $E'$ <sup>(7)</sup>, eq. (3.3) can be written in the form:

$$\frac{d}{dt} N(\nu_0, t) = [\exp(-2\pi\nu/K_B T) - 1] A(\nu, t) N(\nu_0, t) + 8\pi\nu^2 R^2 R_0 \exp(-2\pi\nu/K_B T) A(\nu, t) \quad (3.4)$$

where  $T$  is the radiation temperature at the instant  $t$ . The solution of this equation has the form

$$N(\nu_0, t) = \exp[-\tau(t_1, t)] N(\nu_0, t_1) + 8\pi\nu_0^2 R_0^3 \int_{t_1}^t dt' \exp[-\tau(t', t)] \exp[-2\pi\nu(t')/K_B T(t')] A(\nu(t'), t') \quad (3.5)$$

where  $t_1$  is the time at which initial conditions are taken and



$$\tau(t_a, t_b) = \int_{t_a}^{t_b} dt [1 - \exp(-2\pi\nu(t)/K_B T(t))] A(\nu(t), t) \quad (3.6)$$

is the optical depth at time  $t_b$  for a photon emitted at time  $t_a$ . The first term in the r.h.s. of eq. (3.5) accounts for the photons emitted at time  $t_1$  which are still present at time  $t > t_1$ ; the second one gives the number of photons emitted by the medium from  $t_1$  until the instant  $t$ , with the effects of absorption and induced emission taken into account.

The present spectrum of the CMB follows from eq. (3.5) by taking  $t = t_o$ . No photons are left if we take  $t_1 = 0$ . Let  $\nu_o = \nu$ , then:

$$\rho_\gamma(\nu) d\nu = 2\pi\nu n_\gamma(\nu, t_o) d\nu \quad (3.7)$$

and then

$$\rho_\gamma(\nu) d\nu = 16\pi^2 \nu^3 d\nu \int_0^{t_o} dt \frac{d}{dt} \left\{ \exp[-\tau(t, t_o)] \right\} \left\{ \exp[2\pi\nu(t)/K_B T(t)] - 1 \right\}^{-1} \quad (3.8)$$

Note that if

$$\frac{\nu(t)}{T(t)} = \frac{\nu_o R_o}{T(t)R(t)} \quad (3.9)$$

is independent of time, that is, if

$$T(t) R(t) = \text{constant} \quad (3.10)$$

then this leads to the following equation:

$$\rho_\gamma(\nu) d\nu = \frac{16\pi^2 \nu^3 d\nu}{\exp(2\pi\nu/K_B T_0) - 1} \quad (3.11)$$

and the energy distribution of the CMB will be a blackbody at temperature  $T_0$ . Moreover, this blackbody spectrum holds at any  $t$ , before, during and after recombination.

Let us now examine the condition (3.10). The density and pressure of the thermal component (ideal gas in thermal equilibrium with the radiation) are given by

$$\rho = m_B n_B + a T^4 + (\gamma-1)^{-1} n_B K_B T \quad (3.12)$$

$$P = n_B K_B T + \frac{1}{3} a T^4 \quad (3.13)$$

where  $\gamma$  is the specific heat ratio of the gas. The conservation equation

$$T^{\mu\nu}{}_{;\mu} = 0 \quad (3.14)$$

holds separately for the thermal component. Taking for it an energy-momentum tensor which has a perfect fluid form (see eq. (1.20)), with  $\rho$  and  $P$  given by (3.12) and (3.13) respectively, this conservation equation can be expressed as:

$$\frac{d \ln R}{d \ln T} = - \frac{\sigma + \frac{1}{3}(\gamma-1)^{-1}}{\sigma + 1} \quad (3.15)$$

where

$$\sigma \equiv \frac{4}{3} \frac{a T^4}{n_B K_B T} = \frac{2\pi^4}{45\xi(3)} \eta^{-1} \quad (3.16)$$

is the photon entropy per baryon. Eq. (3.15) ensures the condition (3.10) provided that  $\sigma \gg 1$  at temperature  $T$ . Light element abundance observations imply that, at  $T \approx 1$  MeV, (see Chapter 4)

$$\eta \in [3, 10] \times 10^{-10} \quad (3.17)$$

and we know that  $\eta$  remains constant in an adiabatically expanding universe once  $e^+e^-$  pairs annihilate. We conclude that  $\sigma(T) \gg 1$  for every  $T$  if light elements were synthesized in the early universe. Models with  $\sigma \gg 1$  are known as hot big-bang models.

### 3.1.2 OBSERVATIONS

Measurements of the CMB spectrum carried out in the seventies showed discrepancies between the longwave side, which could be well fitted by a blackbody at temperature  $T = 2.72 \pm 0.08$  K<sup>(8)</sup>, and the region of the maximum, where departures from a blackbody shape were apparent<sup>(9)</sup>.

More recent measurements<sup>(10,11,12)</sup> show that no significant distortion near the peak exists, and that the CMB spectrum is consistent with a blackbody at temperature  $T = 2.75$  K with an accuracy of about 1 percent<sup>(4)</sup> between 0.1 and 12 cm. Figure 3.1 displays the data and their fit.

The fact that no outstanding spectral distortions have been found restricts the models which have been proposed to explain it. In particular, this allows us to bound the parameters of any unstable particle which gives rise to photons as it decays (see Chapter 6).

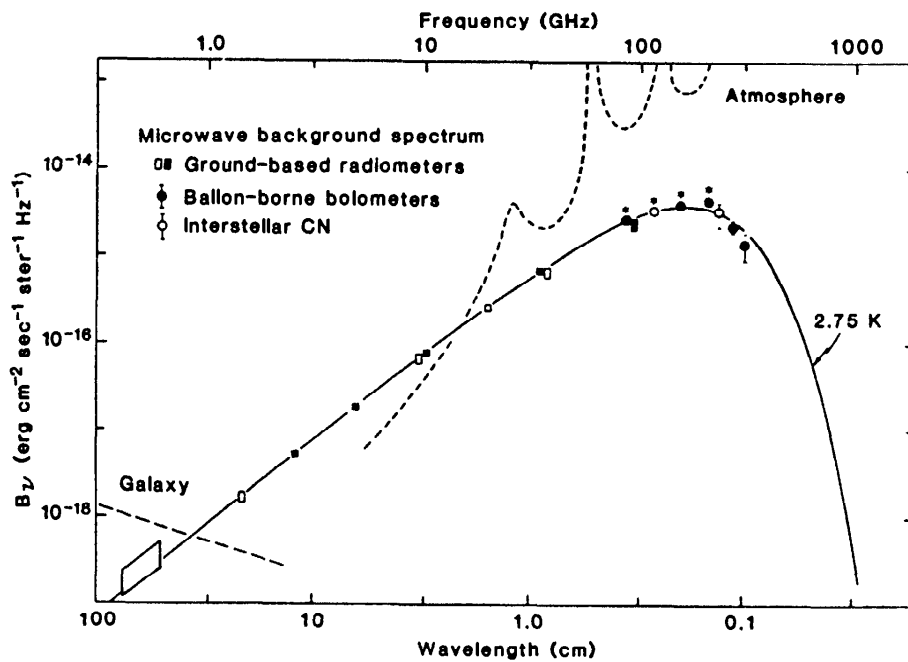


**Figure 3.1** Measures of the surface brightness  $B_\nu$  of the CMB. The spectrum of a 2.75 K blackbody emitter is also shown. Filled squares and circles are recent results. Open squares are old results included for comparison. Open circles represent astronomical measures of interstellar cyanogen (CN) molecules used as thermometers. Asterisks indicate that the symbol is larger than the error bar (from Wilkinson (17); published by the American Association for the Advancement of Science; copyright 1986 by the AAAS).

## 3.2 ANGULAR DISTRIBUTION OF THE MICROWAVE BACKGROUND RADIATION

The possible anisotropies of the microwave background radiation (and their absence) are of major importance as a source of information about the origins of the CMB and also about the physical conditions prevailing in the universe at the epoch in which matter and radiation last interacted. Up to the present, the only anisotropy unambiguously detected is the dipole anisotropy, which can be easily interpreted as being due to the peculiar velocity of the Solar System with respect to the reference frame in which the CMB is perfectly isotropic. While the lack of anisotropy correlated with the Milky Way geometry is a proof of the extragalactic origin of the CMB, its impressive isotropy on small angular scales demonstrates that it does not come from extragalactic radio sources and this implies that the last scattering surface was extremely uniform. This results in very stringent restrictions on the possible large scale structure formation scenarios. Moreover, the absence of large scale anisotropy excludes any anisotropic cosmological model<sup>(13)</sup>, except those in which the anisotropy is only a perturbation<sup>(14)</sup>.

The theoretical aspects of the small scale anisotropy of the CMB related to the evolution of inhomogeneities will be discussed in Chapter 5. Here we will consider the dipolar component interpretation and the horizon problem.

### 3.2.1 THE PECULIAR VELOCITY OF THE OBSERVER

Let us assume that there exists a reference frame in which the CMB is perfectly isotropic and has a Planckian spectrum. In this

frame, the energy-momentum tensor for the radiation can be written thus (see Chapter 1)

$$T^{\mu\nu} = \int \pi_\gamma p^\mu p^\nu N_\gamma(x^\rho, p^\lambda) \quad (3.18)$$

where the photon distribution function in this frame is

$$N_\gamma(x^\rho, p^\lambda) = [\exp(-\beta_\lambda p^\lambda) - 1]^{-1} \quad (3.19)$$

with

$$\beta_\lambda = -u_\lambda / K_B T \quad (3.20)$$

and the photon four-momentum is given by

$$p^\lambda = 2\pi\nu(1, \sin\theta\cos\phi, \sin\theta\sin\phi, \cos\theta) \quad (3.21)$$

The spectral distribution of energy  $\rho_\gamma(\nu, T)$  is such that

$$\int_0^\infty \rho_\gamma(\nu, T) d\nu = T^{00}(T) \quad (3.22)$$

and is independent of the direction of observation in this frame.

Let us now consider an observer with peculiar velocity  $\vec{v}_0$  and a reference frame in which this observer is at rest. In this new frame, the energy-momentum tensor is calculated through an expression similar to (3.18) with

$$N'_\gamma(x'^\rho, p'^\lambda) = [\exp(-\beta'_\lambda p'^\lambda) - 1]^{-1} = N_\gamma(x^\rho, p^\lambda) \quad (3.23)$$

and

$$p'^{\rho} = \Lambda_{\lambda}^{\rho} p^{\lambda} = 2\pi\nu'(1, \sin\theta' \cos\phi', \sin\theta' \sin\phi', \cos\theta') \quad (3.24)$$

where  $\Lambda_{\lambda}^{\rho}$  stands for the Lorentz transformation with velocity  $\vec{v} = -\vec{v}_0$ . In particular, we have the following transformations:

$$\nu' = \nu \frac{(1 - v_0 \cos\theta)}{(1 - v_0^2)^{1/2}} \quad (3.25)$$

$$\cos\theta' = \frac{-v_0 + \cos\theta}{1 - v_0 \cos\theta} \quad (3.26)$$

where  $\theta(\theta')$  is the angle formed by  $\vec{v}_0$  and  $\vec{p}(\vec{p}')$ ,  $\nu'$  is the photon frequency in the new frame and  $(\theta', \phi')$  defines the photon direction (observation direction) in the new frame. The equality

$$\beta_{\lambda} p^{\lambda} = \beta'_{\lambda} p'^{\lambda} \quad (3.27)$$

which holds under the Lorentz transformation given by  $\Lambda_{\lambda}^{\rho}$ , and eqs. (3.20) and (3.21) imply that

$$\frac{2\pi\nu}{K_B T} = -\beta'_{\lambda} p'^{\lambda} \equiv \frac{2\pi\nu'}{K_B T'} \quad (3.28)$$

This defines a temperature  $T'$ , which in accordance with eq. (3.25) is given by

$$T' = \frac{T[1 - v_0 \cos\theta]}{(1 - v_0^2)^{1/2}} \quad (3.29)$$

that is, in each direction the spectral distribution of the energy is still a blackbody, but the blackbody temperature depends on the direction of observation. For practical purposes,  $v_0$  is the peculiar velocity of the Sun, and  $v_0 \ll 1$ , so that eqs. (3.26) and (3.29) lead to:

$$T' \approx T(1 - v_0 \cos\theta') = T + \Delta T(\theta') \quad (3.30)$$

with a correcting term which is independent of frequency and has an angular dependence with a 24-hr period. The effect will be maximum when  $\cos\theta' = 1$ , that is the observation is made in the direction (or the opposite) in which the observer moves. The measurement of  $\Delta T(\theta')$  gives us information about the magnitude and direction of  $\vec{v}_0$ : the peculiar velocity of the Sun with respect to the frame in which the CMB is exactly isotropic can be derived from these measurements (see below).

### 3.2.2 THE HORIZON PROBLEM

Let us consider an observer placed at the origin of a reference system in a FRW geometry, whose radial and time coordinates are  $r = 0$  and  $t$ , respectively. If  $t_1$  is an instant previous to  $t$ ,  $t_1 < t$ , the observer can only receive at time  $t$  signals emitted at time  $t_1$  in points such that the radial coordinate  $r$  verifies  $r < r_1$ , where  $r_1$  is such that a light signal emitted in  $r_1$  at time  $t_1$  reaches the observer in  $r = 0$  at time  $t$ , that is:



$$\int_0^{r_1} \frac{dr}{\sqrt{1-kr^2}} = \int_{t_1}^t \frac{d\tau}{R(\tau)} \quad (3.31)$$

If the integral on the r.h.s. diverges for  $t_1 \rightarrow 0$ , then the observer can receive, at time  $t$ , signals emitted by any comoving particle in the universe, provided that we consider early enough emitting times. If, on the contrary, this integral does not diverge, then at time  $t$  only signals emitted inside a finite region of proper radius

$$d_H(t) = R(t) \int_0^t \frac{d\tau}{R(\tau)} \quad (3.32)$$

can be received by the observer. This defines what is known as a horizon<sup>(15)</sup>. In FRW models,  $R(\tau) \sim \tau^{1/2}$  as  $\tau \rightarrow 0$ , and consequently they have horizons.

The cosmic background radiation we observe nowadays consists of photons which last scattered at time  $t_R$ , where  $t_R$  is the (last) recombination time. The size of the region a light signal can travel from  $t=0$  to  $t=t_R$  is the horizon at  $t_R$ . If the universe homogenization takes place through energy and momentum transport at velocities smaller than  $c$ , then a region whose size exceeded  $2d_H(t_R)$  at time  $t_R$ , would not have had time to erase its possible initial inhomogeneities, and then the CMB would be irregular on angular scales  $\theta > \theta_H$ , where  $\theta_H$  is the angle formed at present by the trajectories of two photons emitted at recombination at two points separated by a proper distance of  $2d_H(t_R)$ . It is given by<sup>(5)</sup>

$$\sin \frac{\theta_H}{2} = \frac{q_o (2q_o z_R + 1)^{1/2}}{z_R q_o + (q_o - 1) [(2q_o z_R + 1)^{1/2} - 1]} \quad (3.33)$$

where

$$1 + z_R = \frac{R_o}{R(t_R)}$$

is the red-shift of the photons emitted at  $t_R$ . If  $z_R \approx 1500$ , then

$$\theta_H \approx 4.2^\circ \sqrt{q_o} \quad (3.34)$$

but the important result is that, for any  $z_R$  and  $q_o$  values, a finite value of  $\theta_H$  is predicted.

No such anisotropies have been clearly observed, and we may then conclude that the hypersurface  $t_R = \text{constant}$ , formed by causally disconnected regions, was homogeneous: this is the horizon problem. A possible homogenization mechanism is provided by inflation<sup>(16)</sup> (see Chapter 8).

### 3.2.3 OBSERVATIONS

#### i) Small scale anisotropies.

No anisotropies in the cosmic background radiation have been compellingly detected on small scales. Only upper limits measured on different scales are available. Figure 3.2 summarizes these upper limits<sup>(17)</sup>. The most stringent and sensitive bound has been obtained

by Usón and Wilkinson<sup>(18)</sup> at  $\theta = 4'.5$ . They quote an upper limit of

$$\frac{\Delta T}{T} \lesssim 2.1 \times 10^{-5} \quad (3.35)$$

(see, however, Kaiser and Silk<sup>(18)</sup>).

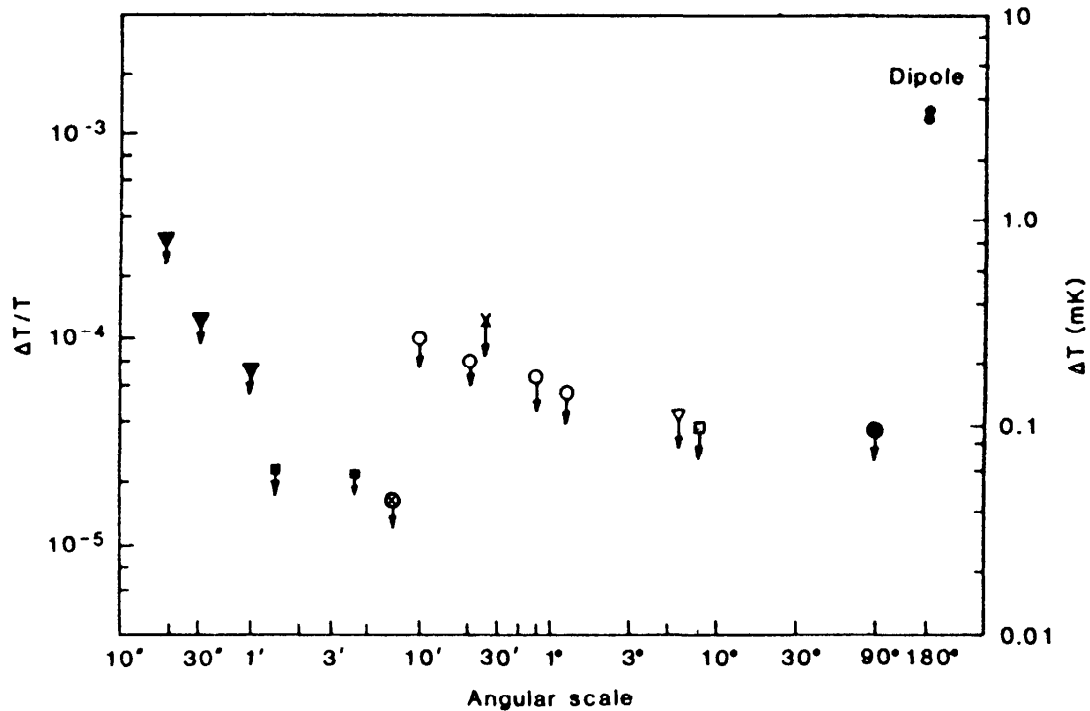


Figure 3.2 Current results of searches for anisotropy in the CMB on all angular scales.  $\Delta T$  is the fluctuation of the CMB temperature. Symbols indicate the sources of the data: ■ reference (18); ▼ reference (19); ○ reference (20); x reference (21); ▽ reference (22); □ reference (23); ● reference (24); • reference (28) (from Wilkinson (17); published by the American Association for the Advancement of Science; copyright 1986 by the AAAS).

The results of the experiments on scales of  $6^\circ$  and  $8^\circ$  can be taken as either an upper limit or a detection, depending on whether they contain or not an uncertain galactic contribution.

ii) Dipole and quadrupole anisotropy.

A dipole component has been measured by several groups: Results of the different research teams are given in the following Table

Table 1

Research group	Dipole amplitude (mK)	R. A. (hours)	Declination (degrees)	Wavelength
Berkeley <sup>(25)</sup>	$3.46 \pm 0.17$	$11.3 \pm 0.1$	$-6.0 \pm 1.4$	3 mm
Princeton <sup>(26)</sup>	$3.18 \pm 0.17$	$11.2 \pm 0.1$	$-8 \pm 2$	1.2 cm
Florence <sup>(27)</sup>	$2.9 \pm 1.3$ $- 0.6$	$11.4 \pm 0.7$	$3 \pm 10$	
MIT <sup>(8)</sup>	$2.8 \pm 0.8$	$9.6 \pm 1.5$	$-9 \pm 20$	
Moscow <sup>(28)</sup>	$3.16 \pm 0.12$	$11.3 \pm 0.15$	$-7.5 \pm 2.5$	8 mm

The most accurate measurements have been done by the Berkeley, Princeton and Moscow groups at different frequencies. Their agreement on the dipole amplitude and direction is surprisingly good. The independence of frequency is necessary if the dipole anisotropy is to be interpreted in terms of the peculiar velocity of the observer. In accordance with these data, the Sun moves with a velocity of  $360 \text{ km s}^{-1}$  toward the constellation Leo. By subtracting the known velocity of the Sun with respect to the galactic center, we obtain a galactic velocity of  $600 \pm 50 \text{ km s}^{-1}$  toward galactic longitude  $265^\circ$  and galactic latitude  $25^\circ$ , toward the constellation Hydra, in a direction which forms an angle of about  $45^\circ$  with the Virgo cluster direction.

The quadrupole component has not yet been detected. The most restrictive upper limits have been obtained from the Soviet satellite

Prognoz-9 measurements at a wavelength of  $\lambda = 8 \text{ mm}$  (point in the figure 3.2 at  $90^\circ$ ) (28)

$$\Delta T \lesssim 10^{-4} \text{ K} \quad (3.36)$$

## REFERENCES 3

1. A.A. Penzias and R.W. Wilson, *Ap. J.* 142 (1965) 419.
2. G. Gamow, *Phys. Rev.* 70 (1946) 572.  
R.A. Alpher, H. Bethe and G. Gamow, *Phys. Rev.* 73 (1948) 803.  
R.A. Alpher and R.C. Herman, *Rev. Mod. Phys.* 22 (1950) 153.
3. R.H. Dicke, P.J.E. Peebles, P.G. Roll and D.T. Wilkinson, *Ap. J.* 142 (1965) 414.
4. R.B. Partridge, 1987, in IAU Symposium No. 124 "Observational Cosmology", A. Hewitt, G. Burbidge and Li Zhi Fang eds. (Dordrecht: Reidel).
5. S. Weinberg, 1972, "Gravitation and Cosmology" (New York: J. Wiley & Sons).
6. P.J.E. Peebles, 1971, "Physical Cosmology" (Princeton: Princeton University Press).
7. L.I. Schiff, 1968, "Quantum Mechanics" (New York: McGraw-Hill).
8. R. Weiss, *Ann. Rev. Astron. Astrophys.* 18 (1980) 489.
9. D.P. Woody and P.L. Richards, *Phys. Rev. Lett.* 42 (1979) 925; *Ap. J. Lett.* 248 (1981) 18.
10. D.M. Meyer and M. Jura, *Ap. J. Lett.* 276 (1984) L1.  
P. Crane, D.J. Hegyi, N. Mandolesi and A.C. Danks, *Ap. J.* 309 (1986) 822.
11. J.B. Peterson, P.L. Richards and T. Timusk, *Phys. Rev. Lett.* 55 (1985) 232.
12. G.F. Smoot ., *Ap. J. Lett.* 291 (1985) L23.
13. M.A.H. Mac Callum and G.F.R. Ellis, *Commun. Math. Phys.* 19 (1976) 31.
14. M.P. Ryan and L.C. Shepley, 1975, "Homogeneous Relativistic Cosmologies" (Princeton: Princeton Univ. Press).
15. W. Rindler, *M.N.R.A.S.* 116 (1956) 663.
16. A.H. Guth, *Phys. Rev.* D23 (1981) 347.  
A.D. Linde, *Phys. Lett.* 108B (1982) 389.  
A. Albrecht and P.J. Steinhardt, *Phys. Rev. Lett.* 48 (1982) 1220.
17. D.T. Wilkinson, *Science* 232 (1986) 1512.
18. J. Usón and D.T. Wilkinson, *Nature* 312 (1984) 427; *Ap. J. Lett.* 277 (1984) L1.  
N. Kaiser and J. Silk, *Nature* 324 (1986) 529.
19. J.E. Knoke, R.B. Partridge, M.I. Ratner and I.I. Shapiro, *Astron. J.* 284 (1984) 473.  
E.B. Fomalont, K.I. Kellerman, J.V. Wall, *Ap. J. Lett.* 277 (1984) L23.
20. Y.N. Parijskij, Z.E. Petrov, L.N. Cherkov, *Sov. Astron. Lett.* 3 (1977) 263.  
A.N. Lasenby and R.D. Davies, *M.N.R.A.S.* 203 (1983) 1137.
21. N. Caderni ., *Phys. Rev.* D16 (1977) 2424.
22. F. Melchiorri, B. Melchiorri, C. Ceccarelli and L. Pietranera, *Ap. J. Lett.* 250 (1981) L1.
23. R.D. Davies ., *Nature* 326 (1987) 462.
24. A. Readhead ., 1987, in IAU Symposium No. 130 "Evolution of Large Scale Structures in the Universe", J. Audouze and A. Szalay eds. (Dordrecht: Reidel).
25. P.M. Lubin, G.L. Epstein and G.F. Smoot, *Phys. Rev. Lett.* 50 (1983) 616.  
P.M. Lubin, T. Villela, G. Epstein and G.F. Smoot, *Ap. J. Lett.* 298 (1985) L1.
26. D.J. Fixsen, E.S. Cheng and D.T. Wilkinson, *Phys. Rev. Lett.* 50 (1983) 620.
27. R. Fabbri, I. Guidi, F. Melchiorri and V. Natale, *Phys. Rev. Lett.* 44 (1980) 1563.
28. I.A. Strukov and D.P. Skulachev, *Sov. Astron. Lett.* 10 (1984) 1.

## CHAPTER 4

### THE STANDARD BIG-BANG NUCLEOSYNTHESIS

In the preceding Chapters it was emphasized that the standard Friedmann-Robertson-Walker (FRW) cosmologies explain, in rather a natural way, the Hubble law and the microwave background of thermal radiation at 2.7 K. In the present Chapter we will discuss a new piece of evidence in support of the big-bang model: the consistency between theory and observations in regard to the abundances of the light elements D,  $^3\text{He}$ ,  $^4\text{He}$  and  $^7\text{Li}$ .

The recession of galaxies and the background radiation provide us with information on the evolution of the universe up to the recombination era, that is, up to  $\approx 10^5$  years after the big-bang. Light element abundances allow us to go back in time until epochs as remote as about  $10^2$  sec. This is the reason why the study of primordial nucleosynthesis (PN) is of major importance in order to decipher the physical conditions in the early universe, and to set up important limits on several astrophysical and particle physics parameters (see

Chapter 6). It must be stressed that the microphysics involved in the PN process (Fermi theory of weak interactions and analytical fittings to measured nuclear cross-sections) is well known.

In the frame of FRW models, the theoretical PN calculation is a closed problem. There remain some uncertainties in the nuclear cross-sections, which result in controlled uncertainties in the predictions of the light element yields. The open question is the evaluation of primordial abundances from the observed ones, and the determination of these observed abundances. An enormous amount of work has been devoted in the recent years to the measurement of light element concentrations in different astronomical sites, and to the understanding of the evolutionary processes which allow us to extrapolate back in time from the present observations up to the big-bang.

#### 4.1 THE PRIMORDIAL NUCLEOSYNTHESIS PROCESS IN STANDARD COSMOLOGIES

The simplest models of PN, such as those first investigated by Peebles<sup>(1)</sup> and Wagoner, Fowler and Hoyle<sup>(2)</sup>, have been constructed in the framework of standard big-bang models which are defined by the following assumptions: i) General Relativity describes correctly the evolution of the universe, ii) the universe was isotropic and homogeneous at PN time, iii) the baryon number asymmetry was present at the epoch of PN, and antibaryon annihilation had been completed at



this time, and iv) the leptonic number is much lower than unity.

During the epoch of relevance for primordial thermonuclear reactions ( $10^{-2} \text{ sec} < t < 10^3 \text{ sec}$  or  $10^{11} \text{K} > T > 4 \times 10^8 \text{K}$ ) the universe is made of photons ( $\gamma$ ), neutrinos ( $\nu$ ) and antineutrinos ( $\bar{\nu}$ ), electrons ( $e^-$ ) and positrons ( $e^+$ ) and nucleons (N: neutrons (n) and protons (p)). As we will see, the nucleon to photon ratio is very low:

$$\eta = \frac{n_N}{n_\gamma} \sim 10^{-9} \quad (4.1)$$

and at this time nucleons are dynamically irrelevant: they are only a trace constituent of the cosmic soup.

In order to describe the nucleosynthesis process, we will first examine the time evolution of the neutron-to-proton abundance ratio. This is controlled by the weak interaction reactions:



which change neutrons into protons and conversely.

Defining the ratio of neutrons and protons to all nucleons by:

$$X_n = \frac{n_n}{n_N} \quad (4.5)$$

and

$$X_p = \frac{n_p}{n_N} \quad (4.6)$$

where  $n_i$  stands for the number density of class  $i$  constituent, we see that  $X_n + X_p = 1$ , and then the kinetic equation describing the  $X_n$  evolution can be written as:

$$\frac{dX_n}{dt} = -\lambda(n \rightarrow p)X_n + \lambda(p \rightarrow n)(1 - X_n) \quad (4.7)$$

where  $\lambda(n \rightarrow p)$  and  $\lambda(p \rightarrow n)$  are the total transition rates for the weak processes which transform neutrons into protons, and protons into neutrons, respectively. They are calculated in the framework of the Fermi theory of weak interactions, and are given by<sup>(3)</sup>:

$$\begin{aligned} \lambda(n \rightarrow p) = C \int dq \left[ 1 - \frac{m_e^2}{(Q+q)^2} \right]^{\frac{1}{2}} (Q+q)^2 q^2 \left[ 1 + \exp\left[ \frac{q}{K_B T_\nu} \right] \right]^{-1} \times \\ \times \left[ 1 + \exp\left[ -\frac{Q+q}{K_B T} \right] \right]^{-1} \end{aligned} \quad (4.8)$$

and:

$$\begin{aligned} \lambda(p \rightarrow n) = C \int dq \left[ 1 - \frac{m_e^2}{(Q+q)^2} \right]^{\frac{1}{2}} (Q+q)^2 q^2 \left[ 1 + \exp\left[ -\frac{q}{K_B T_\nu} \right] \right]^{-1} \times \\ \times \left[ 1 + \exp\left[ \frac{Q+q}{K_B T} \right] \right]^{-1} \end{aligned} \quad (4.9)$$

where

$$Q = m_n - m_p = 1.293 \text{ MeV} \quad (4.10)$$

$m_i$  means the mass of the  $i$  constituent and  $C$  is a normalizing constant, which should be taken in such a way that the half-life for neutron beta decay (eq. (4.4)) coincides with its measured value,  $\tau_n$ .

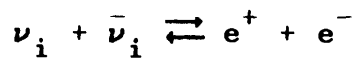
The main qualitative features of the evolution of  $X_n$  may be outlined without numerically integrating eq. (4.7); they are as follows:

i) Let us assume that the universe age at temperature  $T$  is  $t(T)$ . Then, as long as  $\lambda(T) t(T) \gg 1$ , the weak current processes (4.2), (4.3) and (4.4) maintain the neutron abundance at its equilibrium value

$$X_n \approx \frac{\lambda(p \rightarrow n)}{\lambda(p \rightarrow n) + \lambda(n \rightarrow p)} \quad (4.11)$$

This is correct in standard big-bang models with  $N_\nu = 3$  up to a temperature  $T_* \approx 1 \text{ MeV}$  (freezing-out temperature).

ii) All the light neutrinos are kept in equilibrium with  $e^\pm$  by means of the neutral current weak processes:



where  $i = e, \mu, \tau \dots$  Electron neutrinos also have charged current interactions (4.2) - (4.4) so that they decouple slightly later than the other neutrino species. As long as the  $e$  neutrinos are in equilibrium with the thermal component, that is, if  $T = T_\nu$  in eq. (4.8) and (4.9), the rates verify:

$$\frac{\lambda(p \rightarrow n)}{\lambda(n \rightarrow p)} = \exp[-Q/K_B T] \quad (4.12)$$

and then:

$$X_n = \left[ 1 + \exp(Q/K_B T) \right]^{-1} \quad (4.13)$$

which implies that  $X_n(T) \rightarrow 1/2$  for  $K_B T \gg Q$ . This gives the initial condition for (4.7), which follows from the microphysical theory of weak interactions and does not depend on the particular cosmological model describing the evolution of the early universe.

The neutron-to-proton abundance ratio follows from eq. (4.13): for  $T > T_*$

$$\left. \frac{X_n}{X_p} \right|_T = \exp[-Q/K_B T] \quad (4.14)$$

When the temperature drops to  $T < T_*$ , the charged processes (4.2) - (4.4) become too slow and they are no longer able to maintain the equilibrium. Neutrons are heavier than protons, and can still be converted into them, but this process has a low rate. The neutron-to-proton ratio freezes out at  $T_*$ : from  $T \leq T_*$  up to the onset of the nuclear reactions, few neutrons are converted into protons and then:

$$\left. \frac{X_n}{X_p} \right|_T \approx \left. \frac{X_n}{X_p} \right|_{T_*} = \exp[-Q/K_B T_*] \quad (4.15)$$

Let us now consider the nuclear reactions leading to complex

nuclei formation.

Baryon number density is too low to allow for many-body collisions, so that nuclei have to be synthesized by sequences of two-body processes. The first step is to build up deuterium (D):



and only if D is abundant enough, the following steps can proceed. Because the deuteron is very weakly bound and is very easily photodissociated by photons (which we recall, are much more abundant than nuclei), this will happen only when the universe is cool enough that the process:



does not overcome the D formation. The number of thermal photons per nucleon able of photodesintegrating the deuteron varies as:

$$\left. \frac{n_\gamma}{n_N} \right]_D \propto \eta^{-1} \exp[-E_D/K_B T] \quad (4.18)$$

where  $E_D = 2.225$  MeV is the threshold energy for the reaction (4.17). We see that for  $T < T_D^\gamma \approx 0.1$  MeV, D concentration increases, and finally a temperature is reached (whose value depends on  $\eta$ ) such that D is abundant enough and the nucleosynthesis process starts.

Tritium (T) is synthesized via the  $D(n, \gamma)T$  and  $D(D, p)T$  reactions, and helium-3 ( ${}^3\text{He}$ ) by  $D(p, \gamma){}^3\text{He}$  and  $D(D, n){}^3\text{He}$ . These nuclei are burned to helium-4 ( ${}^4\text{He}$ ) through  $T(p, \gamma){}^4\text{He}$ ,  $T(D, n){}^4\text{He}$ ,  ${}^3\text{He}(n, \gamma){}^4\text{He}$ ,  ${}^3\text{He}(D, p){}^4\text{He}$ ,  ${}^3\text{He}({}^3\text{He}, 2p){}^4\text{He}$ , while the process  ${}^3\text{He}(n, p)T$

changes  ${}^3\text{He}$  into T and conversely. These are the main processes leading to  ${}^4\text{He}$  synthesis. Every present nuclear species interact with the remaining nuclei, leading to a rather complicated network of nuclear reactions<sup>(4)</sup>.

To have a quantitative picture of the synthesis process in the big-bang, one must carry out a numerical integration of the equations of nuclear reaction kinetics resulting from this network:

$$\frac{dY_i}{dt} = \pm \sum \lambda_j Y_j \pm \sum \beta_{jk} Y_j Y_k \quad (4.19)$$

where  $Y_i = n_i/n_N$  is the fraction by number of the  $i$  nuclide, the sums include all the processes leading to  $i$  formation (sign +) or destruction (sign -), and  $\lambda_j$  and  $\beta_{jk}$  are their respective rates. This integration was first carried out by Peebles (1966)<sup>(1)</sup>, Wagoner, Fowler and Hoyle (1967)<sup>(2)</sup> and Wagoner (1969)<sup>(4)</sup>, who first considered a nuclear reaction network including all elements with mass number  $A \leq 32$ . The method to determine the rates is the standard one in Nuclear Astrophysics; a detailed discussion of this subject can be found in two papers by Fowler, Caughlan and Zimmerman (1967)<sup>(5)</sup> and updated versions in the papers by Fowler, Caughlan and Zimmerman (1975)<sup>(6)</sup> and by Harris et al. (1983)<sup>(7)</sup>.

As the universe cools, fewer and fewer nuclei are able to surmount the Coulomb barriers, and the nuclear rates decrease as a consequence of this. For  $T < 4 \times 10^8 \text{K}$ , the thermonuclear reactions become ineffective, and the PN process is completed. No more nuclear activity occurs until the first generation of stars form.

The outcome of all these nuclear reactions is the incorporation

of almost all available neutrons into  ${}^4\text{He}$ , which has the highest binding energy by nucleon of all light nuclei. The reason is that the Coulomb barrier in the reactions  ${}^4\text{He}({}^3\text{He}, \gamma){}^7\text{Be}$  and  ${}^4\text{He}(T, \gamma){}^7\text{Li}$ , and the absence of stable nuclei with  $A=5$  and  $A=8$ , prevent  ${}^4\text{He}$  destruction. Each  ${}^4\text{He}$  nucleus is formed by two neutrons and two protons so that its mass fraction at the end of the PN,  $Y_p$ , can be estimated to be:

$$Y_p \approx 2 X_n(T_D^\gamma) \approx 2 X_n(T_*) \approx 0.25 \quad (4.20)$$

and in the first approximation does not depend on the nucleon density. The other light element production in the early universe is much lower, and can only be known through numerical integration of eqs. (4.19).

#### 4.2 PREDICTED ABUNDANCES AND THEIR UNCERTAINTIES

In the standard big-bang models the light element final yields depend on the neutron half-life,  $\tau_n$ , the number of light neutrino families,  $N_\nu$ , and the present baryon density, which is usually expressed in terms of the baryon-to-photon ratio  $\eta$ . The main qualitative traits of the PN computations outcome in these kind of models have not been altered since Wagoner's 1973 work<sup>(8)</sup>. They are the following:

i) Only D,  ${}^3\text{He}$ ,  ${}^4\text{He}$  and  ${}^7\text{Li}$ , (Lithium-7) are significantly produced in the big-bang.

ii) The  ${}^4\text{He}$  abundance does not appreciably depend on the baryon density. On the contrary, D,  ${}^3\text{He}$  and  ${}^7\text{Li}$  final yields are remarkably sensitive to the parameter  $\eta$ .

iii) The  ${}^4\text{He}$  production is an increasing function of  $\tau_n$  and  $N_\nu$ , while other nuclei production is almost insensitive to these parameters.

Figure 4.1 shows the theoretical light element abundances as functions of the  $\eta$  parameter. For  ${}^4\text{He}$  we show the results for  $N_\nu = 2, 3$  and 4 with  $\tau_n = 10.6$  min; the error bars correspond to the typical variations in  $Y_p$  when the neutron half-life is taken to be  $\tau_n = 10.4$  min and  $\tau_n = 10.8$  min instead of  $\tau_n = 10.6$  min. These PN yields have been taken from Schramm<sup>(9)</sup> and Yang et al.<sup>(10)</sup>. The most eminent features of this figure are the steep decrease in the D and D plus  ${}^3\text{He}$  abundances as  $\eta$  grows, the valley shape of the  ${}^7\text{Li}/\text{H}$  versus  $\eta$  curve<sup>1</sup>, with steep slopes on both sides of the minimum, and the rather slow increase of  $Y_p$  with the baryon number (notice the difference of scales used in figure 4.1 for  ${}^4\text{He}$  and the other elements).

The behavior of the D and  ${}^3\text{He}$  abundances can be understood on the basis of the D and  ${}^3\text{He}$  burning to  ${}^4\text{He}$  with rates  $\propto \eta$ , which results in a lower survival of these elements as  $\eta$  increases. The observed  ${}^7\text{Li}$  is the sum of the  ${}^7\text{Li}$  and the  ${}^7\text{Be}$  synthesized in the big-bang. For low baryon densities ( $\eta_{10} \equiv \eta/10^{10} \lesssim 3$ ),  ${}^7\text{Li}$  is mainly produced through the  ${}^4\text{He}(T, \gamma){}^7\text{Li}$  reaction and destroyed via  ${}^7\text{Li}(p, \alpha){}^4\text{He}$ . As  $\eta$  grows, this last process becomes more and more

---

<sup>1</sup>In what follows, we will use the notation  $E_1/E_2$  to mean  $N(E_1)/N(E_2)$  where  $N(E)$  is the atom number density of the element E.



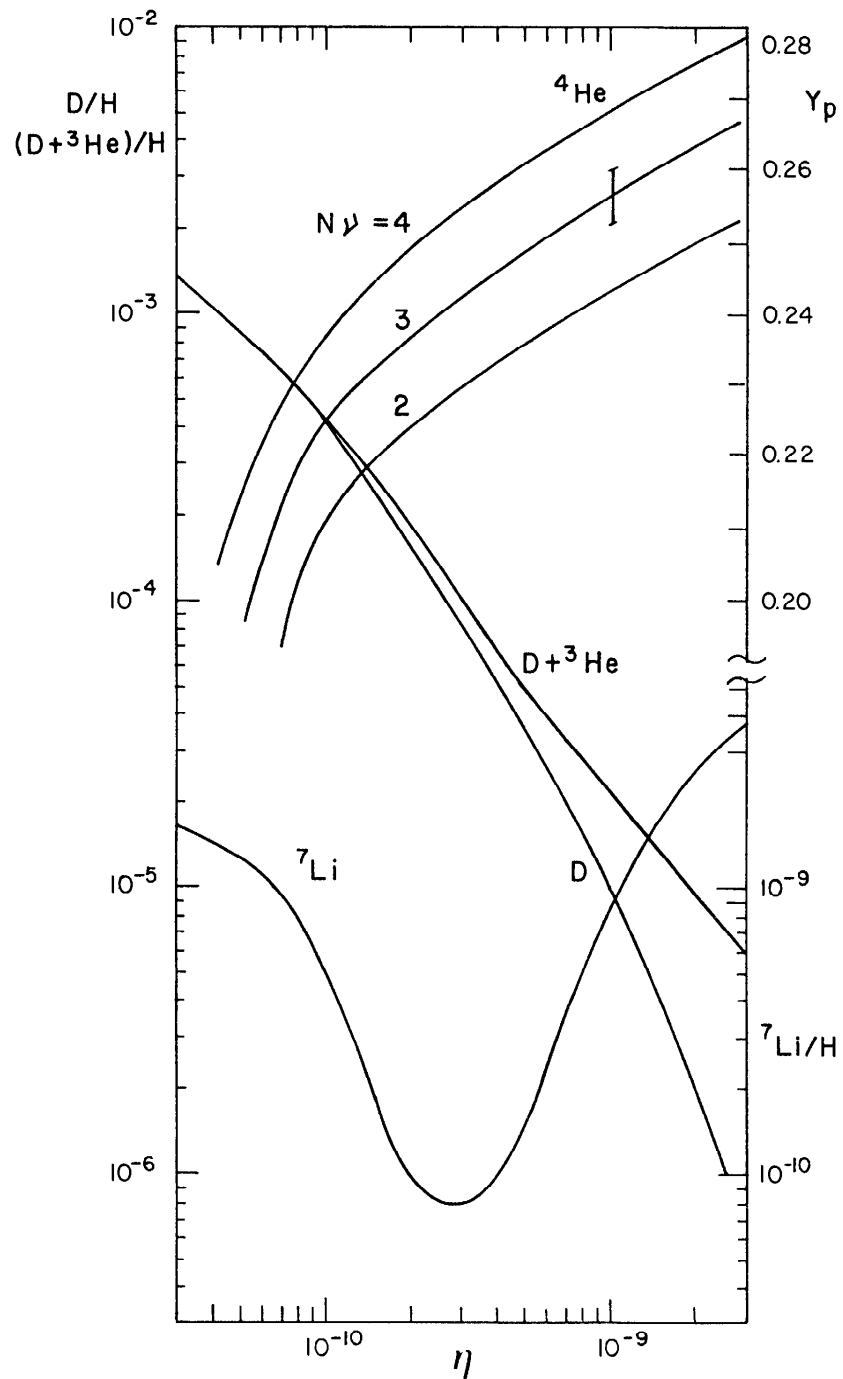


**Figure 4.1** Light element yields as functions of the  $\eta$  parameter. For  ${}^4\text{He}$ , the mass fraction  $Y_p$  is shown, while for D,  ${}^3\text{He}$  and  ${}^7\text{Li}$ , the abundances by number relative to H are given (see text).

important, and finally it overcomes the production reaction and closes this pathway. But then another possibility arises: For  $\eta_{10} \gtrsim 3$ ,  ${}^7\text{Li}$  is formed by  ${}^4\text{He}({}^3\text{He}, \gamma){}^7\text{Be}$ , whose rate increases with  $\eta$ . The competition among these three reactions determines the minimum in the  ${}^7\text{Li}$  abundance curve.

${}^4\text{He}$  production is an increasing function of the freezing-out temperature  $T_*$  (see eq. (4.15) and (4.20)), which is roughly determined by the condition:

$$\lambda(T_*) t(T_*) = 1 \quad (4.21)$$

The higher  $N_\nu$  (or, in general, the higher the effective number of relativistic degrees of freedom,  $g_{\text{eff}}$ ) is considered and the faster the universe expands. Eq. (1.90) gives the universe age at temperature  $T$  as:

$$t(T, g_{\text{eff}}) \propto g_{\text{eff}}^{-1/2} T^{-2} \quad (4.22)$$

On the other hand, the weak interaction rate can be written as:

$$\lambda(T) = n \sigma_{\text{wk}} v \quad (4.23)$$

where  $n \propto T^3$  and  $\sigma_{\text{wk}} \propto T^2$ . Since the  $C$  constant in eqs. (4.8) and (4.9) is  $C \propto \tau_n^{-1}$ ,  $\lambda(T)$  varies as:

$$\lambda(T, \tau_n) \propto \tau_n^{-1} T^5 \quad (4.24)$$

Eqs. (4.21), (4.22) and (4.24) now give:

$$T_* \propto \left[ g_{\text{eff}}^{1/2} \tau_n \right]^{1/3} \quad (4.25)$$

and hence the  $Y_p$  behavior with respect to  $N_\nu$  and  $\tau_n$ .

Even if only slightly,  $Y_p$  increases with  $\eta$ . This is due to the neutron transformation into protons between  $T_*$  and the beginning of the thermonuclear reactions at  $T_N$ . This temperature range is smaller for higher  $\eta$  (see eq. (4.18)), and therefore fewer neutrons are converted into protons, which results in a higher  ${}^4\text{He}$  production.

All these behavior patterns can be summarized in the analytical expression<sup>(11)</sup>:

$$Y_p = 0.230 + 0.011 \ln \eta_{10} + 0.013(N_\nu - 3) + 0.014(\tau_n(\text{min}) - 10.6) \quad (4.26)$$

which correctly fits the  ${}^4\text{He}$  mass fraction produced in the big-bang for  $1.5 < \eta_{10} < 10$ .

A key point when assessing the PN as a method of testing the early universe is knowing the uncertainties in the predicted abundances due to uncertainties in the nuclear rates entering the equations of nuclear reaction kinetics<sup>(10,12,13)</sup>. The calculated yields are known to within an accuracy of less than a few percent in the case of D and  ${}^3\text{He}$ , and less than 1% in the case of  $Y_p$ . This is much less than the uncertainties in the observations (see Section 4.3). The situation is different with regard to  ${}^7\text{Li}$  production. The main uncertainties lie in the  ${}^7\text{Li}(p,\alpha){}^4\text{He}$  reaction (a factor of about 2<sup>(10)</sup>) at low  $\eta$ , and in the  ${}^4\text{He}({}^3\text{He},\gamma){}^7\text{Be}$  process (a factor 2<sup>(14,15)</sup>)

at high  $\eta$ , which imply that the  ${}^7\text{Li}$  yields are uncertain by a factor of about 2. This fact is not critical, however, because the minimum in the  ${}^7\text{Li}/\text{H}$  curve does not change remarkably.

### 4.3 OBSERVED ABUNDANCES

The determination of light element primordial abundances to be compared with the predicted PN production is a difficult open question. It deserves a lot of attention because of the information carried by these abundances on the physics and microphysics of the early universe. In evaluating primordial abundances, there exist two sources of difficulties: the measurement itself, and the extrapolation of what is observed at present up to the PN time. This is particularly true for D and  ${}^3\text{He}$ , whose concentrations at PN time as inferred from astronomical data depend crucially on the details of stellar and galactic evolution<sup>(13,16)</sup>.

Recent extensive and critical reviews on light element abundance observations can be found in Yang et al. (1984)<sup>(10)</sup>, Audouze (1984)<sup>(17)</sup> and Boesgaard and Steigman (1985)<sup>(11)</sup>.

#### 4.3.1 DEUTERIUM

Deuterium is burned to  ${}^3\text{He}$  in the stars and is not additionally produced in stellar evolution. As a consequence, the whole D observed at present has necessarily a cosmological origin and provides a lower

bound on its primordial abundance. Moreover, as shown in figure 4.1, D production is a steep decreasing function of  $\eta$ , so that an upper limit on  $\eta$  can be inferred from its measurement. The cosmological relevance of deuterium abundance determinations results from these two circumstances.

Two main astrophysical sites are suitable for D observations: the Solar System and the interstellar space. The null result of deuterium search in stellar atmospheres leads only to the upper limit  $D/H < 1 \times 10^{-6}$  in Canopus<sup>(18)</sup>.

i) Solar System (abundances in the protosolar nebula, that is, about  $4.5 \times 10^9$  years ago).

During the pre-main sequence phase of the Sun, D was converted into  $^3\text{He}$ , so that the present  $^3\text{He}$  in the solar wind is the sum of presolar D and  $^3\text{He}$  (plus, possibly,  $^3\text{He}$  produced in the Sun). The solar wind has deposited  $^3\text{He}$  in the gas-rich meteorites, the lunar soil and the foil left on the Moon by the Apollo mission, and its abundance can be determined. As an average of different measurements<sup>(19,20)</sup>, Boesgaard and Steigman (1985)<sup>(11)</sup> give:

$$\langle (D+^3\text{He})/^4\text{He} \rangle_{\text{pre}\odot} = (4.0 \pm 0.2) \times 10^{-4} \quad (4.27)$$

In carbonaceous chondrites, D is unprocessed. They have been used by several authors<sup>(20,21)</sup> to estimate  $(^3\text{He}/^4\text{He})_{\text{pre}\odot}$ . A weighted average of all the data leads to the value<sup>(11)</sup>:

$$\langle ^3\text{He}/^4\text{He} \rangle_{\text{pre}\odot} = (1.54 \pm 0.27) \times 10^{-4} \quad (4.28)$$

If  $^3\text{He}$  in the solar wind is not contaminated by solar  $^3\text{He}$ <sup>(22)</sup>, we can infer the presolar abundance of D relative to  $^4\text{He}$  by subtracting (4.28) from (4.27). As an average of all the data, we are led to<sup>(11)</sup>:

$$\langle \text{D}/^4\text{He} \rangle_{\text{pre}\odot} = (2.5 \pm 0.5) \times 10^{-4} \quad (4.29)$$

Taking for the solar  $^4\text{He}$  abundance the value<sup>(11)</sup>:

$$(^4\text{He}/\text{H})_{\odot} = 0.09 \pm 0.01 \quad (4.30)$$

we obtain:

$$(\text{D}/\text{H})_{\text{pre}\odot} = (2.2 \pm 0.7) \times 10^{-5} \quad (4.31)$$

and

$$[(\text{D} + ^3\text{He})/\text{H}]_{\text{pre}\odot} = (3.6 \pm 0.6) \times 10^{-5} \quad (4.32)$$

The molecular ratios  $\text{HD}/\text{H}_2$  and  $\text{CH}_3\text{D}/\text{CH}_4$  in giant planets atmospheres have been used to deduce D/H. It has been argued<sup>(23)</sup> that the abundances determined by this method should be close to the presolar ones. Unfortunately, they depend on the details of the planetary atmosphere models. We quote the following results:

$$\left. \begin{array}{l} \text{Jupiter} \\ \left\{ \begin{array}{l} (\text{D}/\text{H})_{\text{pre}\odot} = \left[ \begin{array}{l} 3.6 + 1.0 \\ - 1.4 \end{array} \right] \times 10^{-5} \quad (24) \\ (\text{D}/\text{H})_{\text{pre}\odot} = (1.2 - 3.1) \times 10^{-5} \quad (25) \\ (\text{D}/\text{H})_{\text{pre}\odot} = \left[ \begin{array}{l} 3.2 + 0.9 \\ - 1.25 \end{array} \right] \times 10^{-5} \quad (26) \end{array} \right. \end{array} \right\} \quad (4.33) \quad (4.34) \quad (4.35)$$

$$\text{Saturn} \quad (D/H)_{\text{pre}\odot} = \left[ \begin{array}{c} 2.4 + 2.4 \\ - 1.3 \end{array} \right] \times 10^{-5} \quad (27) \quad (4.36)$$

These  $(D/H)_{\text{pre}\odot}$  abundances are in good agreement with the indirect determinations in meteorites.

ii) Interstellar gas (abundances found now).

Interstellar D has been detected in the wings of the Lyman lines of HI by means of the Copernicus satellite. Several lines-of-sight toward nearby cool stars and toward more distant hot stars have been used.

In both cases, D/H determinations in the direction of different stars show a big scatter: differences of as much as a factor of more than ten have been obtained in the lines-of-sight to cool stars<sup>(28)</sup>.

Two main difficulties appear in the evaluation of interstellar deuterium toward hot stars: variability in the scale of hours and multiple clouds in the line-of-sight. The former, first detected in the direction of  $\epsilon$  Perseus<sup>(29)</sup> and then confirmed in other stars<sup>(30)</sup>, has been interpreted as being the effect of a high velocity HI transient component ejected by the star. It blends the D lines inducing an apparent increase in the D/H values. Therefore, the true value would be rather low. Vidal-Madjar et al. (1983)<sup>(29)</sup> give:

$$D/H \approx (5 \pm 3) \times 10^{-6} \quad (4.37)$$

The presence of several clouds in the line-of-sight, on the contrary, leads to an underestimation of D/H. These difficulties

suggest that only the cleanest line-of-sight data should be used, in this case the scatter is less important and the resulting D/H toward hot stars has a most probable value of<sup>(11)</sup>:

$$0.8 \times 10^{-5} \leq D/H \leq 2 \times 10^{-5} \quad (4.38)$$

The quality of the data and the reliability of the analysis techniques is lower for the cool stars.

#### 4.3.2 HELIUM 3

<sup>3</sup>He is produced by incomplete hydrogen burning in low mass ( $M < 2M_{\odot}$ ) stars<sup>(31)</sup>. It is also destroyed in the interiors of more massive stars, although some will survive in their outer layers<sup>(32,33)</sup>. Its chemical evolution is quite complicated and it is not clear whether its primordial abundance should be higher than, lower than or of the same order as the abundances observed in the Solar System and in the interstellar medium.

##### i) Solar System.

As previously discussed, the presolar ratio <sup>3</sup>He/<sup>4</sup>He can be directly measured in carbonaceous chondrites. <sup>3</sup>He abundance relative to hydrogen is deduced from (4.28) and (4.30):

$$(^3\text{He}/\text{H})_{\text{pre0}} = (1.4 \pm 0.4) \times 10^{-5} \quad (4.39)$$

##### ii) Interstellar space.



It is possible to detect the interstellar singly ionized  $^3\text{He}$  by observing the 8.7 GHz hyperfine line in HII regions. The line is very weak, however, and the line-to-continuum ratio very small. This makes the detection technically difficult. It was only successfully achieved, after many attempts, in 1984 by Rood et al.<sup>(34)</sup>. They report positive detections in three galactic HII regions: W43 ( $^3\text{He}/\text{H} \approx 4 \times 10^{-5}$ ), W51 ( $^3\text{He}/\text{H} \approx 1 \times 10^{-4}$ ) and W3 ( $^3\text{He}/\text{H} \approx 5 \times 10^{-4}$ ). New observations of these sources and detections in six regions<sup>(35)</sup> give abundances ranges from  $1.2 \times 10^{-5}$  to  $14.7 \times 10^{-5}$ . These values, when compared with the presolar value, suggest that there is a slight tendency to galactic enrichment since the Solar System formation

#### 4.3.3 HELIUM 4

The  $^4\text{He}$  abundance can be determined with much higher precision than the other light element abundances, because of its higher cosmic concentration. This is the reason why  $^4\text{He}$  is a key constraint in physics theories, by comparing in detail PN predictions and data. (Note, however, that, in order to decipher physical conditions at PN time,  $^4\text{He}$  abundance must be known within an error of less than  $\pm 5\%$ <sup>(11)</sup>). Many observations have been made in different astrophysical sites (Sun and Solar System, young and old star atmospheres, globular clusters, planetary nebulae, HII regions in our own and other galaxies, and isolated intergalactic HII regions). For an excellent discussion on  $^4\text{He}$  abundance, see references (36) and (37).

Galaxies increase their  $^4\text{He}$  content throughout their evolution, because of stellar processing. As a consequence, to derive the

primordial  ${}^4\text{He}$  concentration,  $Y_p$ , either unevolved objects, an enrichment model or an extrapolation device are needed.

This last method has been employed to determine  $Y_p$  from the recombination emission lines of HeI and HeII in HII regions, with different metal content (that is, in different stages of chemical evolution). A correlation between  $Y$  and the metallicity  $Z$  would be expected on the basis of current evolution models, so that an extrapolation toward  $Z=0$  would give the pregalactic  ${}^4\text{He}$  content. Nevertheless, at present the observational situation is uncertain. While some authors find this correlation<sup>(38)</sup>, no evidence for an unambiguous correlation is found by other observers<sup>(39)</sup>. Among these last, Kunth and Sargent's (1983) results are most often adopted. They have studied 12 metal-poor low-luminosity galaxies and give, for a weighted mean of the  ${}^4\text{He}$  abundance in those 12 galaxies:

$$Y_p \leq 0.245 \pm 0.003 \quad (4.40)$$

They have taken  $Z$  to be proportional to the O/H content and conclude that the possible correlation between  $Y$  and  $Z$  is lost in the error bars for low  $Z$ .

Pagel et al. (1986)<sup>(40)</sup> have recently analysed a sample of blue compact galaxies selected in such a way that the correction for (unobservable) neutral  ${}^4\text{He}$  be negligible. They claim for a lower  $Y_p$  value:

$$Y = (0.238 \pm 0.005) + (2.9 \pm 1.5)Z \quad (4.41)$$

(1  $\sigma$  error). Now:

$$Z = 10^3 N/H$$

Steigman et al.<sup>(41)</sup> have studied the correlation between helium and carbon. They derive a central value of

$$Y_p = 0.235 \tag{4.42}$$

in agreement with Pagel et al. Given the scatter in the  $Y$  values for HII regions, the uncertainty in  $Y_p$ ,  $\Delta Y_p$ , should be larger than those given in equations (4.40) and (4.41) above.

Davidson and Kinman (1985)<sup>(42)</sup> have done an analysis of  $Y$  in the object I Zw 18, which is the most metal poor of the blue compact galaxies. They have paid particular attention to all the sources of error, and conclude that

$$Y_p = 0.23 \pm 0.01 \tag{4.43}$$

Gautier et al.<sup>(43)</sup> have derived the  $^4\text{He}$  content on the surface of Jupiter from Voyager data. They found:

$$0.17 \leq Y \leq 0.24 \tag{4.44}$$

These limits are reliable as long as a differentiation of helium from hydrogen has not occurred in the Jovian atmosphere<sup>(44)</sup>.

The spectral lines of HeI and HeII are only detected in the atmospheres of hot O and B stars, which are of the youngest type, so that their  $^4\text{He}$  content represents the results of stellar processing by

previous generations of stars. Comparison of theoretical line profiles with observed ones gives<sup>(45)</sup>

$$Y = 0.28 \pm 0.04 \quad (4.45)$$

Globular clusters are old objects. Their <sup>4</sup>He content can therefore be expected to be only primordial. There exist, however, many uncertainties in the methods of deducing Y from their observation. Buzzoni et al. (1983)<sup>(46)</sup> have obtained:

$$Y = 0.23 \pm 0.02 \quad (4.46)$$

Determinations of  $Y_p$  from planetary nebulae are very model dependent. Peimbert (1983)<sup>(47)</sup> has found

$$Y_p \approx 0.22 \quad (4.47)$$

We conclude that primordial <sup>4</sup>He is more reliably known from observations of HII regions, which produce the smallest errors among all the available methods. The best current data imply:

$$0.23 \leq Y_p \leq 0.25 \quad (4.48)$$

but values in the range

$$0.22 \leq Y_p \leq 0.26 \quad (4.49)$$

cannot be rejected at present.

#### 4.3.4 LITHIUM 7

${}^7\text{Li}$  is destroyed in the inner layers of the stars which are hot enough for  $(p,\alpha)$  reactions to occur. Lithium in the stellar atmospheres is diluted if these interior regions are mixed with the surface of the star, through convective and diffusive processes.

Spite and Spite (1982)<sup>(48)</sup> and Spite et al. (1984)<sup>(49)</sup> have measured  ${}^7\text{Li}/\text{H}$  at the surface of a sample of 25 very old halo stars. On the basis of statistical arguments (independence of  ${}^7\text{Li}$  abundance on stellar mass, in contrast with the expected behavior if mixing had taken place<sup>(50)</sup>), these authors maintain that lithium has not been diluted in the atmosphere of these stars, and because they are Population II stars, their determination corresponds to the primordial  ${}^7\text{Li}$  content. They give:

$${}^7\text{Li}/\text{H} = (0.7 - 1.8) \times 10^{-10} \quad (4.50)$$

Spallation reactions on C, N and O nuclei in the interstellar gas caused by galactic cosmic rays could produce Li, Be and B isotopes<sup>(51)</sup>. The amount of  ${}^7\text{Li}/\text{H}$  formed would be about  $2 \times 10^{-10}$  ( $\sim 30\%$  of which is  ${}^6\text{Li}$ ). Neither  ${}^6\text{Li}$  nor Be has been found in halo stars up to now<sup>(52)</sup>, what suggests that no Li so produced is present in Population II stars.

Observations of Hyades, Pleiades and field stars evidence that Population I stars exhibit a constant upper limit of the  ${}^7\text{Li}/\text{H}$  abundance<sup>(53)</sup>:

$${}^7\text{Li}/\text{H} \leq 10^{-9} \quad (4.51)$$

which was thought to be the primordial concentration until Spite and Spite's measurements.

It is difficult to decide which one of the values (4.50) or (4.51) represents the primordial value. In the first case, a homogeneous enrichment along galactic evolution by a factor of 10 would be needed. Production in red giants and novae have been invoked as a possible source of stellar  ${}^7\text{Li}$ . In the second hypothesis, the uniform depletion of lithium in halo stars has to be explained.

Because of these uncertainties, it is usual to take<sup>(11)</sup>:

$$0.7 \times 10^{-10} \leq ({}^7\text{Li}/\text{H})_p \leq 8 \times 10^{-10} \quad (4.52)$$

the upper limit resulting from the maximum value found in Population I stars once the product of spallation reactions has been subtracted.

#### 4.4 PRIMORDIAL ABUNDANCES AND CONSISTENCY THEORY/ASTRONOMICAL DATA

From the preceding Section we conclude that  ${}^4\text{He}$  and  ${}^7\text{Li}$  can be observed in astronomical sites (respectively low metallicity extragalactic HII regions, and Population II stars or Population I stars, when their maximum  ${}^7\text{Li}$  content is considered to be the primordial  ${}^7\text{Li}$  abundance) where chemical evolution has played a minor or even negligible role in regard to the abundance of these elements.

Consequently, the  ${}^4\text{He}$  and  ${}^7\text{Li}$  primordial concentrations can be deduced from their measurements in these unevolved objects.

D and  ${}^3\text{He}$  abundances, on the contrary, can only be determined from regions largely affected by galactic evolution: the Solar System and the interstellar medium. Two approaches are then possible concerning their primordial abundances: either to estimate limits on them or to infer their value through detailed models of chemical galactic evolution.

The first kind of method has been adopted by the Chicago group<sup>(10,11)</sup>, who only consider lower limits on  $(\text{D}/\text{H})_p$  directly provided by observations, (because no post big-bang D production is possible), and evaluate upper bounds on  $[(\text{D}+{}^3\text{He})/\text{H}]_p$ .

The Solar System data on D suggest that (eqs. (4.31) and (4.33) - (4.36)):

$$(\text{D}/\text{H})_p \geq (1-2) \times 10^{-5} \quad (4.53)$$

which in turn implies (see figure 4.1):

$$\eta_{10} \leq 10^{-7} \quad (4.54)$$

It is also possible to place an upper limit on the primordial abundance of D plus  ${}^3\text{He}$ , once the fraction of  ${}^3\text{He}$  which survives stellar processing,  $g$ , is known. In fact, assume that  $f$  is the fraction, at time  $t$ , of the interstellar gas which has not suffered astration. Then

$$(D/H)_t = f(D/H)_p \quad (4.55)$$

and

$$({}^3\text{He})_t \geq f ({}^3\text{He})_p + g(1-f) (D+{}^3\text{He})_p \quad (4.56)$$

The second term on the r.h.s. of eq. (4.56) takes into account the fraction of primordial  ${}^3\text{He}$  (plus primordial D burned to  ${}^3\text{He}$  in stars), which survives stellar destruction.  ${}^3\text{He}$  production in low mass stars is difficult to quantify: it has been neglected and hence the inequality in eq. (4.56). Eqs. (4.55) and (4.56) lead to:

$$\left[ \frac{D+{}^3\text{He}}{H} \right]_p \leq \left[ \frac{D+{}^3\text{He}}{H} \right]_t + \left[ \frac{1}{g} - 1 \right] \left[ \frac{{}^3\text{He}}{H} \right]_t \quad (4.57)$$

An accurate calculation of  $g$  requires knowing the initial mass function (IMF) for the earliest generation of stars. For a Salpeter<sup>(54)</sup> IMF, Yang et al.<sup>(10)</sup> estimate that:

$$g \geq 1/2 \quad (4.58)$$

and  $g \geq 1/4$  if the estimate is made on a star-by-star basis (safe bet value). This result has been confirmed by more detailed calculations<sup>(33)</sup>.

${}^3\text{He}$  destruction might have been more important in the first generation of stars if the weight of massive stars had been more important than that given by Salpeter's IMF (as would be the case if the IMF depended on the metallicity, for example).

Taking for D and  ${}^3\text{He}$  their presolar abundances (4.32) and



(4.39), eq. (4.57) gives

$$\left[ \frac{D+{}^3\text{He}}{\text{H}} \right]_{\text{p}} \leq 6.0 \times 10^{-5} \quad \text{if } g \geq 1/2 \quad (4.59)$$

and

$$\left[ \frac{D+{}^3\text{He}}{\text{H}} \right]_{\text{p}} \leq 9.6 \times 10^{-5} \quad \text{if } g \geq 1/4 \quad (4.60)$$

These upper bounds imply a lower limit on  $\eta$  (see figure 4.1):

$$\eta_{10} \geq 4 \quad \text{if } g \geq 1/2 \quad (4.61)$$

or:

$$\eta_{10} \geq 3 \quad \text{if } g \geq 1/4 \quad (4.62)$$

As for  ${}^7\text{Li}$  observations, the upper limit in eq. (4.52) and figure 4.1 give:

$$0.8 \leq \eta_{10} \leq 10 \quad (4.63)$$

these values are consistent with those deduced from D and  ${}^3\text{He}$  observations. The consistency persists when the uncertainty factor in  ${}^7\text{Li}$  production is taken into account.

We are thus led to a safe bet interval of  $\eta_{10}$  values where D,  ${}^3\text{He}$  and  ${}^7\text{Li}$  are produced in agreement with observations:

$$3 \leq \eta_{10} \leq 10 \quad (4.64)$$

For the standard scenario with three light neutrino families and  $\tau_n = 10.6$  min, the primordial  ${}^4\text{He}$  production in this interval is:

$$0.243 \leq Y_p \leq 0.255 \quad (4.65)$$

which is coherent with primordial  ${}^4\text{He}$  abundance determinations from astronomical data (eq. (4.48)) once the uncertainties are considered. However, if future work confirms the present tendency to lower  $Y_p$  values, then this consistency picture could be in trouble. For example, taking Pagel et al.'s  $Y_p$  value (and error bars, eq. (4.41)), only if the uncertainties in primordial D plus  ${}^3\text{He}$  and  ${}^4\text{He}$  are stretched to their limits does the agreement persist. In this case<sup>(55)</sup>:

$$3 \leq \eta_{10} \leq 3.6 \quad (4.66)$$

unless  ${}^3\text{He}$  destruction in massive stars has been more important than what is commonly thought<sup>(10,33)</sup>, and  $g < 1/4$ , or there exist only two families of light neutrinos.

The alternative approach concerning the inference of primordial abundances is provided by modelling the chemical evolution of the Galaxy. These models, for light elements of cosmological relevance, have been developed by J. Audouze and co-workers in France. Standard models of galactic evolution<sup>(56)</sup> give a rather low factor for D destruction due to stellar processing:

$$\frac{D_p}{D_{\text{now}}} \approx 2 - 3 \quad (4.67)$$

In this framework, if  $Y_p \leq 0.24$  and  $N_\nu = 3$ , there would be an inconsistency between  ${}^4\text{He}$  and the interstellar D measurements (eq. (4.38)), mainly if we consider the determination of Vidal-Madjar et al. (eq.(4.37)) as the actual value (see figure 4.1).

In order to surmount this difficulty, non standard models of galactic evolution have been proposed by the French group<sup>(13,16,57)</sup>: the D destruction ratio may be considerably increased when the effect of infall or inflow of processed material on the evolution of chemical concentrations is considered. Two possibilities exist i) an infall of D free material, either extragalactic or coming from other regions of the Galaxy, and ii) the mass-loss of D free material by stars during their pre-main sequence phase. With this kind of models it is possible to reconcile an interstellar D value as low as  $D/H \sim 5 \times 10^{-6}$  with a solar system abundance of  $D/H \sim 3 \times 10^{-5}$  and a primordial concentration of  $D/H \sim 10^{-4}$ . The  ${}^3\text{He}$  enrichment of the interstellar medium depends on its production rate in low mass stars, and solutions may be found which are compatible with observations. These authors propose as primordial abundances:

$$3 \times 10^{-5} \leq \left[ \frac{D}{H} \right]_p \leq 2 \times 10^{-4} \quad (4.68)$$

$$9 \times 10^{-6} \leq \left[ \frac{{}^3\text{He}}{H} \right]_p \leq 3 \times 10^{-5} \quad (4.69)$$

which result in the following permissible range of  $\eta_{10}$  values:

$$1.2 \leq \eta_{10} \leq 4.5 \quad (4.70)$$

This is consistent with  ${}^7\text{Li}$  and  ${}^4\text{He}$  primordial values. Non-standard

specific models of galactic evolution are then required in order for the standard big-bang light element yields to be compatible with observations, if  $Y_p \leq 0.24$  and  $N_\nu = 3$ .

## REFERENCES 4

1. P.J.E. Peebles, *Ap. J.* 146 (1966) 542.
2. R.V. Wagoner, W.A. Fowler and F. Hoyle, *Ap. J.* 148 (1967) 3.
3. S. Weinberg, 1972, "Gravitation and Cosmology" (New York: J. Wiley & Sons).
4. R.V. Wagoner, *Ap. J. Suppl.* 18 (1969) 247.
5. W.A. Fowler, G.R. Caughlan, and B.A. Zimmerman, *Ann. Rev. Astron. Astrophys.* 5 (1967) 525.
6. W.A. Fowler, G.R. Caughlan, and B.A. Zimmerman, *Ann. Rev. Astron. Astrophys.* 13 (1975) 69.
7. M.J. Harris, W.A. Fowler, G.R. Caughlan and B.A. Zimmerman, *Ann. Rev. Astron. Astrophys.* 21 (1983) 165.
8. R.V. Wagoner, *Ap. J.* 179 (1973) 343.
9. D.N. Schramm, *Phil. Trans. Roy Soc. A* 307 (1982) 43.
10. J. Yang, M.S. Turner, G. Steigman, D.N. Schramm and K.A. Olive, *Ap. J.* 281 (1984) 493.
11. A.M. Boesgaard and G. Steigman, *Ann. Rev. Astron. Astrophys.* 23 (1985) 319.
12. G. Beaudet and H. Reeves, 1983, in "Proceedings of the ESO Workshop on Primordial Helium". P.A. Shaver, D. Kunth and K. Kjar eds. (Garching: ESO).
13. P. Delbourgo-Salvador, C. Gry, G. Malinie and J. Audouze, *Astron. Astrophys.* 150 (1985) 53.
14. H. Kräwinkel et al., *Z. Phys.* A304 (1982) 307.
15. J.L. Osborne et al., *Nucl. Phys.* A419 (1984) 115.
16. P. Delbourgo-Salvador, Thèse, Université Paris 7 (1986).
17. J. Audouze, 1984, in "Large Scale Structure of the Universe, Cosmology and Fundamental Physics". G. Setti and L. Van Hove, eds. CERN Publications.
18. M. Peimbert, G. Wallerstein and C.A. Pilachowski, *Astron. Astrophys.* 104 (1981) 72.  
R. Ferlet, M. Dennefeld, and M. Spite, *Astron. Astrophys.* 124 (1983) 172.
19. J. Geiss and H. Reeves, *Astron. Astrophys.* 18 (1972) 126.
20. P.M. Jeffrey and E. Anders, *Geochim. Cosmochim. Acta* 34 (1970) 1175.  
D.C. Black, *Geochim. Cosmochim. Acta* 36 (1972) 347.
21. U. Frick and R.K. Moniot, 1977, in *Proc. 8th Lunar Sci. Conf.*  
P. Eberhardt, 1978, in *Proc. 9th Lunar Sci. Conf.*
22. E. Schatzman and A. Maeder, *Astron. Astrophys.* 96 (1981) 1.
23. W.B. Hubbard and J.J. MacFarlane, *Icarus* 44 (1980) 676.
24. V. Kunde et al., *Ap. J.* 263 (1982) 443.
25. T. Encrenaz and M. Combes, *Icarus* 52 (1982) 54.
26. D. Gautier, 1983, in "Proceedings of the ESO Workshop on Primordial Helium", *op. cit.*
27. R. Courtin, Thèse, Université Paris 7 (1982).
28. A. Vidal-Madjar and C. Gry, *Astron. Astrophys.* 138 (1984) 285.
29. A. Vidal-Madjar, C. Laurent, C. Gry, P. Bruston, R. Ferlet and D.G. York, *Astron. Astrophys.* 120 (1983) 58.
30. C. Gry, H.J.G.L.M. Lamers and A. Vidal-Madjar, *Astron. Astrophys.* 137 (1984) 29.
31. J. Iben, Jr., *Ap. J.* 147 (1967) 624.
32. D.S.P. Dearborn, J.B. Blake, K.L. Hainebach and D.N. Schramm, *Ap. J.* 223 (1978) 552.
33. D.S.P. Dearborn, D.N. Schramm and G. Steigman, *Ap. J.* 302 (1986) 35.
34. R.T. Rood, T.M. Bania and T.L. Wilson, *Ap. J.* 280 (1984) 629.
35. T.M. Bania, R.T. Rood and T.L. Wilson, *Ap. J.* in press (1987).
36. B.E.J. Pagel, *Phil. Trans. R. Soc. London A* 307 (1982) 19.

37. P.A. Shaver, D. Kunth and K. Kjar, 1983, eds. "ESO Workshop on Primordial Helium" (Garching: ESO).
38. M. Peimbert and S. Torres-Peimbert, Ap. J. 193 (1974) 327.  
M. Peimbert and S. Torres-Peimbert, Ap. J. 203 (1976) 581.  
J. Lequeux, M. Peimbert, J.F. Rayo, A. Serrano and S. Torres-Peimbert, Astron. Astrophys. 80 (1979) 155.  
H.B. French, Ap. J. 240 (1980) 41.  
M. Peimbert and S. Torres-Peimbert and J.F. Rayo, Ap. J. 220 (1978) 516.
39. R.J. Dufour, Ap. J. 195 (1975) 315.  
D.L. Talent and R.J. Dufour, Ap. J. 233 (1979) 888.  
T.D. Kinman and K. Davidson, Ap. J. 243 (1981) 127.  
D. Kunth, Thèse, Université Paris 7 (1982).  
D. Kunth and W.L.W. Sargent, Ap. J. 273 (1983) 273.  
P.A. Shaver, M.X. Mc Gee, L.M. Newton, A.C. Danks and S.R. Pottash, M.N.R.A.S. 204 (1983) 53.
40. B.E.J. Pagel, R.J. Terlevich and J. Melnick, Pub. Astr. Soc. Pacific, in press.
41. G. Steigman, J.S. Gallagher and D.N. Schramm, (1986), in preparation.
42. K. Davidson and T.D. Kinman, Ap. J. Suppl. 58 (1985) 321.
43. D. Gautier et al, J. Geophys. Res. 86 (1981) 8713.
44. D. Gautier and T. Owen, Nature 302 (1983) 215.
45. P.E. Nissen, 1983, in "Proceedings of the ESO Workshop on Primordial Helium", op. cit.
46. A. Buzzoni, F. Fusi Pecci, R. Buohanno, C.E. Corsi, 1983, in "Proceedings of the ESO Workshop on Primordial Helium", op. cit.
47. M. Peimbert, 1983, in "Proceedings of the ESO Workshop on Primordial Helium", op. cit.
48. F. Spite and M. Spite, Astron. Astrophys. 115 (1982) 357.
49. M. Spite, J.P. Maillard and F. Spite, Astron. Astrophys. 141 (1984) 56.
50. G. Michaud, G. Fontaine and G. Beaudet, Ap. J. 282 (1984) 206.
51. M. Meneguzzi, J. Audouze and H. Reeves, Astron. Astrophys. 15 (1971) 37.
52. E. Maurice, F. Spite, M. Spite, Astron. Astrophys. 132 (1984) 278  
P. Molano, J.E. Beckman, Astron. Astrophys. 139 (1984) 394.
53. R.R. Zappala, Ap. J. 72 (1972) 57.  
D.K. Duncan and B.F. Jones, Ap. J. 248 (1983) 651.  
R. Cayrel, G. Cayrel de Strobel, B. Campbell and W. Dappen, Ap. J. 283 (1984) 205.  
A.M. Boesgaard and M.J. Tripicco, Ap. J. 302 (1986) L49.
54. E.E. Salpeter, Ap. J. 121 (1955) 161.
55. B.E.J. Pagel, preprint "Nucleosynthesis" (1985).
56. J. Audouze and B.M. Tinsley, Ap. J. 192 (1974) 487.
57. C. Gry, G. Malinie, J. Audouze and A. Vidal-Madjar, 1984, in "Formation and Evolution of Galaxies and Large Structures in the Universe", J. Audouze and J. Tran Than Van ed. (Dordrecht: Reidel).

## CHAPTER 5

### THE LARGE SCALE STRUCTURE FORMATION

The problem of the origins of the large scale structure of the universe as observed today is an unsolved one. The standard framework to understand it rests on the hypothesis that it has been formed from quantum fluctuations originated at very high temperatures. These fluctuations evolved in a linear regime until they reached a nonlinear regime at relatively small scales, and then they collapsed giving rise to the bound objects, or to the looser structures we observe nowadays.

The initial spectrum of the perturbations was an initial condition put by hand in the models until the advent of the inflationary paradigm. In this framework, the initial spectrum results in a natural way from first principles (see Chapter 9). A wide class of inflationary models gives rise to a scale invariant spectrum<sup>(1)</sup>.

On the other hand, scenarios leading to a baryon asymmetry<sup>(2)</sup>,

produce only adiabatic perturbations in a natural way. These modes are characterized by a constant entropy through the perturbation. The difficulty in yielding isothermal perturbations (characterized by a homogeneous temperature) has caused authors not to pay much attention to them during the past years.

In this Chapter we consider the essential aspects of the linear perturbation theory and of the cosmological N-body simulations, which describe the nonlinear development of clustering. Their out-puts are to be compared with large scale structure observations. As will be noticed, no simple inflationary scenario fulfils every observational requirements.

## 5.1 CHARACTERISTIC MASSES

The fate of a perturbation in the physical magnitudes which describe the universe in the big-bang model, depends on its scale, for a given composition of the cosmic soup. According to its scale (or mass), a given fluctuation may grow, leading to an instability, oscillate or decay.

The critical mass for the instability appearance is termed Jeans mass,  $M_J$ . In an expanding universe, its value changes with time (or temperature); the form of the function  $M_J(T)$  depends on the scenario considered, that is, on the type of particles contributing to the energy-momentum tensor of the cosmic fluid.



In order to gain insight into the physical processes leading to characteristic masses, we will consider in this Section the Jeans mass for the main scenarios found in the literature, as obtained from crude arguments. A more elegant and precise treatment of this question, is achieved in the framework of the linear analysis of the perturbations to FRW models (see Section 5.3).

### 5.1.1 JEANS MASS FOR A PHOTON, BARYON, ELECTRON AND MASSLESS NEUTRINO GAS

This is the composition of the standard cosmic gas for  $T \lesssim 1$  MeV.

Let us consider a perturbation on scales  $\lambda$  in a medium of density  $\rho$ . It will evolve into an instability if the gravitational energy inside a volume of size  $\lambda^3$  (for example, a sphere of radius  $\lambda$ ) is much greater than its kinetic energy content, that is, if<sup>(3,4)</sup>

$$\frac{G(\rho\lambda^3)^2}{\lambda} \gg \rho v_s^2 \lambda^3 \quad (5.1)$$

where  $v_s$  is the speed of sound in the medium, and, in our case,  $\rho = \rho_b + \rho_e + \rho_\gamma$ . (The fluctuations in the massless neutrino component decay very fast<sup>(5)</sup> and, consequently, this component does not enter the computation of  $\rho$ ). Eq. (5.1) shows that the perturbation grows if its wavelength is longer than

$$\lambda \gg \lambda_J = \left[ \frac{\pi v_s^2}{G\rho} \right]^{1/2} \quad (5.2)$$

where  $\lambda_J$  is termed the Jeans length. As the universe expands,  $\lambda$  grows as  $R(t)$ . It is more convenient to characterize the unstable disturbance by some invariant quantity relative to the universe evolution, such as the fluid mass inside a volume of size  $\lambda_J$ . The baryon Jeans mass is the mass in baryons inside a sphere of radius  $\lambda_J$

$$M_{JB}(T) = \frac{4\pi}{3} n_B(T) m_B \left[ \frac{\pi v_s^2(T)}{G \rho(T)} \right]^{3/2} \quad (5.3)$$

where  $n_B$  and  $m_B$  are the baryon number density and the proton mass, respectively. From the above analysis, we conclude that a given perturbation with mass  $M$  will grow at time  $t$ , when the temperature of the cosmic fluid is  $T$ , if  $M > M_{JB}(T)$ , and will oscillate like a sound wave if  $M < M_{JB}(T)$ . Figure 5.1 displays the temperature behavior of  $M_{JB}$ . Notice the rapid decrease of  $M_{JB}$  for  $T=T_R$ , which is due to the change in the state equation of the fluid as the radiation pressure becomes ineffective at  $T_R$ . Disturbances of galactic masses ( $\approx 10^{11} M_\odot$ ) or greater in the baryon fluid, can only grow when  $T < T_R$ .

### 5.1.2 SILK MASS

Adiabatic fluctuations undergo before  $T_R$  a kind of damping, caused by radiative diffusion, which tends to erase temperature gradients on scales smaller than a critical one. Its translation into a critical mass is known as the Silk mass,  $M_S^{(6)}$ . Let us briefly describe how it is deduced.

A disturbance on scales  $\lambda$  is transparent to radiation if  $\lambda < \lambda_{op} = (\kappa \rho)^{-1}$ , where  $\kappa$  is the fluid opacity due to Thomson scattering

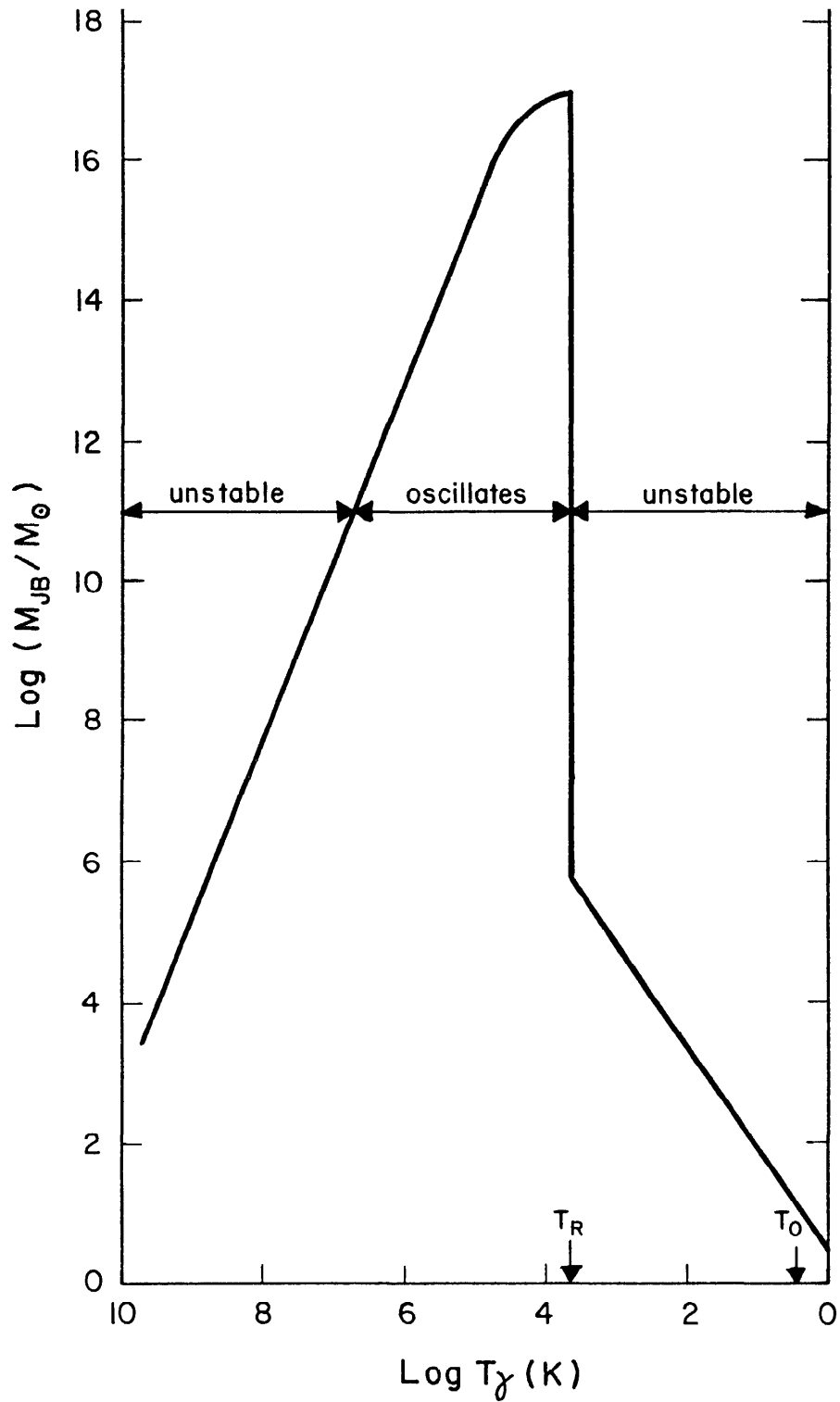


*Figure 5.1 Qualitative behavior of the baryon Jeans mass as a function of the temperature for a typical cosmological model.*

by free electrons. Opaque fluctuations are damped by photon diffusion. A quantitative treatment of the question implies the linearization of the continuity, motion, energy conservation (taking into account the heat flux due to radiative transfer) and field equations. In the framework of the Newtonian approximation, the following equations are obtained:

$$\frac{d^2 \delta_k}{dt^2} + \frac{2\dot{R}}{R} \frac{d\delta_k}{dt} - \left( 4\pi G\rho - \frac{K_B T}{m_B} \frac{4\pi^2}{\lambda^2} \right) \delta_k = - \frac{4aT^4}{3\rho} \frac{4\pi^2}{\lambda^2} \frac{\delta_k T}{T} \quad (5.4)$$

$$\left( \frac{d}{dt} + \frac{\lambda_{op}}{3} \frac{4\pi^2}{\lambda^2} \right) \frac{\delta_k T}{T} = \frac{1}{3} \frac{d\delta_k}{dt} \quad (5.5)$$

with  $\delta_k \left( \frac{\delta_k T}{T} \right)$ , the Fourier component of  $\delta \equiv \frac{\delta\rho}{\rho} \left( \frac{\delta T}{T} \right)$  relative to wavenumber  $k$  and

$$\lambda = \frac{2\pi k}{R} \quad (5.6)$$

the comoving wavelength. In the optically thin case the Jeans condition is recovered. In the optically thick limit an asymptotic treatment of eqs. (5.4) and (5.5) shows that the dominant mode of  $\delta_k$  is damped with a time scale of:

$$t_a \approx \frac{5}{c\lambda_{op}} \frac{\lambda^2}{4\pi^2} \quad (5.7)$$

and the non-damping condition before recombination:

$$\frac{t_R}{t_a} < 1 \quad (5.8)$$

imposes a lower bound to the scales which survive this process of radiative diffusion. This lower bound is the Silk mass:

$$M_S \approx 10^{12} M_{\odot} (\Omega_0 h^2)^{-2} [1 + 0.04 (\Omega_0 h^2)^{-1}]^{-3} \quad (5.9)$$

Fluctuations in the baryonic component on scales  $M < M_S$  are erased before recombination.

A more precise numerical treatment of this problem can be found in references (7,8,9). Damping during recombination leads to<sup>(10)</sup>

$$M_C \approx 10^{16} M_{\odot} \quad (5.10)$$

It has been shown<sup>(11)</sup> that for isothermal perturbations a critical mass exists:

$$M_C \approx 5 \times 10^5 (\Omega_0 h^2)^{-1/2} M_{\odot} \quad (5.11)$$

such that if  $M < M_C$ , the disturbance is damped by photon diffusion. This means that in the isothermal picture, the first scales to go non-linear are smaller than a galactic size. Large scale structure will form by hierarchical clustering of these smaller substructures (bottom-top scenario).

### 5.1.3 JEANS MASS FOR MASSIVE COLLISIONLESS PARTICLES

Fluctuations in a gas of relativistic collisionless particles are damped on scales casually connected, that is smaller than the

horizon, because a (collisionless) relativistic particle X freely streams at velocity c, erasing the inhomogeneities on subhorizon scales.

However, if the X particle is massive, when  $T < T_{NR}$ , where  $K_B T_{NR} = m_X/3.15$ , its thermal velocity is smaller than the light speed, and the perturbation will be able to persist if its mass is larger than a critical mass, which by extension is also termed the Jeans mass for X,  $M_{JX}$ . We will now estimate  $M_{JX}$  following the principles of ref. (12) and (13).

Let us consider a disturbance on scales  $\lambda_k = \frac{2\pi R(t)}{kR_D}$  and the following characteristic times ( $R_D$  is the cosmic scale factor at X decoupling):

i) The average time the particle X takes to cross the perturbation

$$t_{c,X} \approx \lambda_k \langle v^{-1} \rangle \quad (5.12)$$

where

$$\langle v^{-1} \rangle \equiv \langle E_X(p)/p \rangle \quad \text{and} \quad E_X(p) = (p^2 + m_X^2)^{1/2} .$$

ii) The average crossing time for the other components in the cosmic soup (other  $\equiv$  dominant component)

$$t_{c,o} \approx \lambda_k v_{th}^{-1} \quad (5.13)$$

with  $v_{th}$  the thermal velocity of the dominant component.

iii) The dynamical time for the growth of perturbations, in the X component due to its own gravity alone:

$$t_{d,X} \approx \left[ \frac{8\pi G}{3} \rho_X(t) \right]^{-1/2} \quad (5.14)$$

iv) The dynamical time for the growth of perturbations in the X component gravitationally induced by the other components:

$$t_{d,o} \approx \left[ \frac{8\pi G}{3} \rho_{other}(t) \right]^{-1/2} \quad (5.15)$$

A sufficient condition for the appearance of gravitational instability is that the fluctuations in the X component have no time to be erased by free-streaming, that is:

$$t_{c,X} > t_{d,X} \quad (5.16)$$

However, this condition is not necessary because fluctuations may be induced by the other components. The necessary condition reads:

$$t_{c,X} > \min(t_{d,X}, t_{d,o}) \quad (5.17a)$$

provided that

$$t_{c,o} > t_{d,o} \quad (5.17b)$$

which ensures that the disturbances in the other component are not erased. Condition (5.17a) is sufficient to avoid damping in the X component on scales  $\lambda_k$ .

This condition gives the following values for  $M_{JX}(T)$  (see fig. 5.2)

i) At early times X is relativistic (R) and we have a radiation dominated dynamics:

$$M_{JX}(T) = \frac{C_X}{m_X^2} \left[ \frac{1+z_{NR}}{1+z} \right]^3 \quad (5.18)$$

where  $C_X$  is a constant which depends on X and  $z_{NR}$  is the red-shift at which the X particle becomes non relativistic. If X is a neutrino,  $C_\nu \approx 4 \times 10^{17} (\text{eV})^2 M_\odot$ .

ii) At later times X is non-relativistic (NR), and the energy density is provided by baryons or X particles.

$$M_{JX}(T) = \frac{C'_X}{m_X^2} \left[ \frac{1+z}{1+z_{NR}} \right]^{3/2} \min \left[ \left[ \frac{\Omega_X}{\Omega_B} \right]^{3/2}, 1 \right] \quad (5.19)$$

iii) At intermediate epochs, X particles shift from the R to the NR regime, and they become the dynamically dominant component of the cosmic gas. The energy density in the form of X particles can be parametrized by<sup>(13)</sup>

$$\rho_X = \frac{m_X}{2} \tilde{g}_X \left[ \frac{T_X}{T_\gamma} \right]^3 n_\gamma \quad (5.20)$$



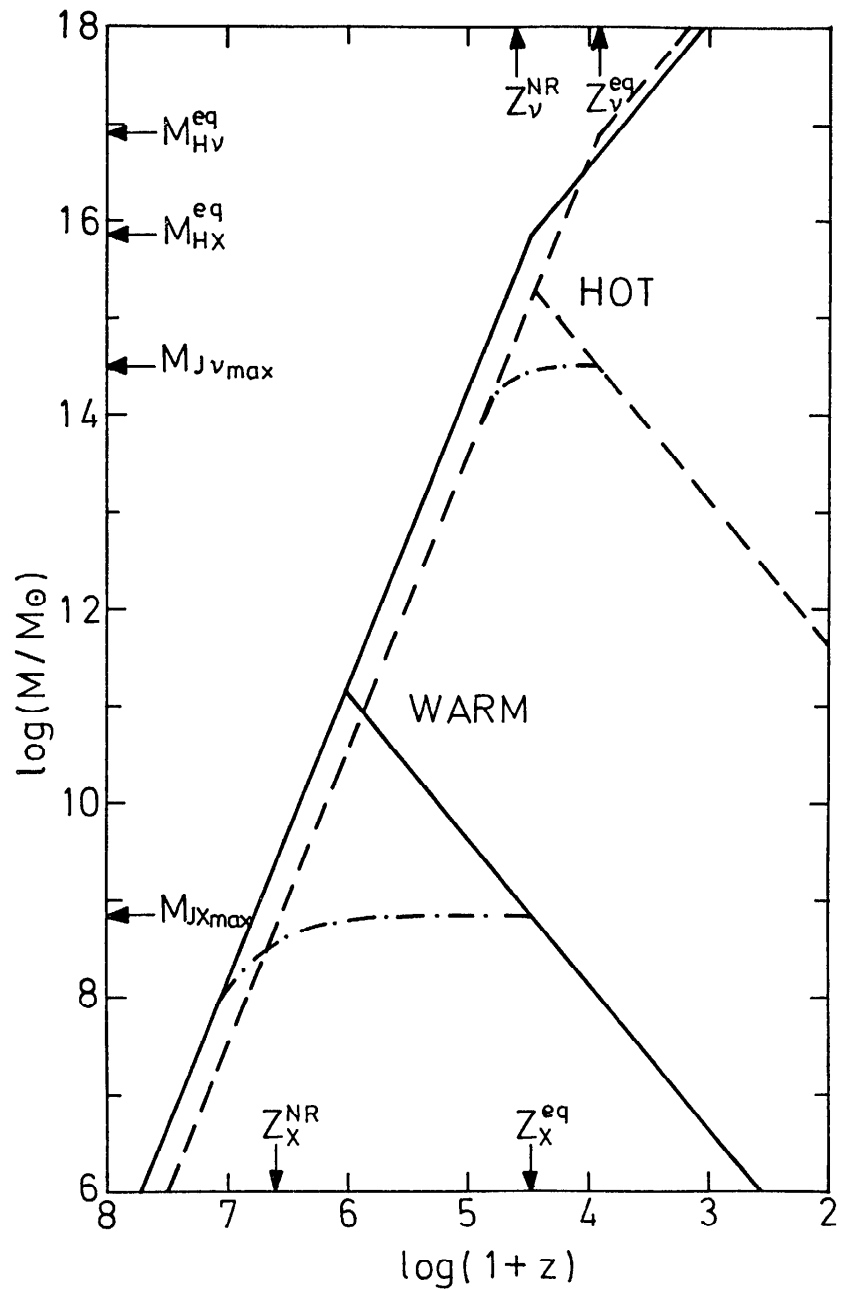


**Figure 5.2** Jeans mass for hot (neutrino) and warm ( $m_X \approx 1$  keV,  $g_{eff}^E(T_{DX}) \approx 100$ ) scenarios as a function of the red-shift. The horizon mass for both scenarios is also shown.

$$\text{where } \tilde{g}_X = \begin{cases} 3/4 g_X & \text{if } X \text{ is a fermion} \\ g_X & \text{if } X \text{ is a boson} \end{cases}$$

and

$$\left( \frac{T_X}{T_\gamma} \right)^3 = \frac{\pi (RT)_{\text{before}}^3}{\text{ann} (RT)_{\text{after}}^3} \quad (5.21)$$

the product including every pair annihilation from X decoupling at  $T_{DX}$  up to T. If the X particle is a neutrino

$$\left( \frac{T_\nu}{T_\gamma} \right)^3 = 4/11 \quad (5.22)$$

and  $\Omega_{\nu 0} \lesssim 1$  implies  $\sum_i m_{\nu_i} \lesssim 100 \text{ eV}$  (hot dark matter).

For  $T_{DX} \gg m_\mu$

$$\left( \frac{T_X}{T_\gamma} \right)^3 = \frac{3.9}{g_{\text{eff}}^E(T_{DX})} \quad (5.23)$$

and  $\Omega_{X0} \lesssim 1$  means that

$$m_X \lesssim 1 \text{ keV} \frac{g_{\text{eff}}^E(T_{DX})}{100} \frac{1.5}{\tilde{g}_X} \quad (5.24)$$

This suggests a dark matter candidate, which would be a very weakly interacting particle of mass  $m_X \approx 1 \text{ keV}$ , so that  $T_{DX} \gg m_\mu$  and

$g_{\text{eff}}^{\text{E}}(T_{\text{DX}}) \approx 100$ . This is the warm dark matter scenario. Gravitinos and photinos have been proposed to satisfy these requirements<sup>(13,14)</sup>, but now masses in excess of 1 GeV are preferred for supersymmetric particles. In this case, their abundance should be suppressed by inflation<sup>(15)</sup>, so as to fit the  $\Omega_{\text{X}0} \approx 1$  condition. This constitutes the cold dark matter scenario. (Axions with a mass of  $10^{-5}$  eV behave as non-relativistic particles, as far as the problem of structure formation is considered, and constitute another candidate for the cold dark matter picture<sup>(16)</sup>).

X particles will dominate the universe dynamics at  $T_{\text{eq}}$  when

$$\rho_{\text{R}}(T_{\text{eq}}) = \rho_{\text{X}}(T_{\text{eq}}) \quad (5.25)$$

which for hot and warm dark matter gives

$$\frac{T_{\text{eq}}}{T_{\text{NR}}} = 6.8 \times 10^{-3} \left[ \frac{g_{\text{eff}}^{\text{E}}(T_{\text{DX}})}{100} \right]^{-4/3} \left[ \frac{1.5}{\tilde{g}_{\text{X}}} \right]^{-1} \quad (5.26)$$

If  $g_{\text{eff}}^{\text{E}}(T_{\text{DX}}) \approx 100$ , we are led to

$$\frac{T_{\text{eq}}}{T_{\text{NR}}} \approx 6.8 \times 10^{-3} \quad (5.27)$$

while for neutrinos we have:

$$\frac{T_{\text{eq}}}{T_{\text{NR}}} \approx 0.23 \quad (5.28)$$

This fact distinguishes the hot and warm scenarios. In the first case, the time interval where radiation dominates the dynamics with NR

X particles is very short; in the second case it is longer. During this interval, fluctuations in the X gas inside their horizon do not grow because perturbations in the baryon-photon fluid oscillate with a time  $t_{c,0} \ll t_{d,0}$ . A scale appears, given by the mass inside the horizon at  $T_{eq}$  which for warm dark matter can be written as<sup>(13)</sup>:

$$M_{HX}^{eq} = 0.9 M_{Pl}^3 m_X^{-2} g_{eff}^E(T_{DX}) \tilde{g}_X^{-2} \quad (5.29)$$

such that the disturbance growth is retarded below  $M_{HX}$ .

Condition (5.17a) results in a value for a maximum Jeans mass  $M_{JX_{max}}$  in this intermediate period given by

$$M_{JX_{max}} = 2.9 M_{Pl}^3 m_X^{-2} g_{eff}^E(T_{DX})^{-2} \tilde{g}_X \quad (5.30)$$

Perturbations on scales  $M < M_{JX_{max}}$  are expected to be damped by free-streaming of the X component.

We see that for warm dark matter two scales arise which are quite different:  $M_{HX}^{eq}$  and  $M_{JX_{max}}$ . Fluctuations on scales  $M < M_{HX}^{eq}$  do not grow until  $T_{eq}$ . As a result, the initial spectrum is expected to be flattened for  $M < M_{HX}^{eq}$ , to be kept for  $M > M_{HX}^{eq}$  and to fall off for  $M < M_{JX_{max}}$ . The same considerations apply in the cold dark matter scenario, except that in this case  $M_{JX_{max}}$  is too tiny to be astrophysically relevant, so that there does not exist a short wavelength cut-off as in the previous cases.

For neutrinos, on the contrary, the scales  $M_{H\nu}^{eq}$  and  $M_{J\nu_{max}}$  are not as different as in the case of warm dark matter (see figure 5.2).

The most striking feature of this scenario is the high value of  $M_{J\nu_{\max}}$ , which roughly corresponds to superclusters (see references (17), (18), (19) and (20)).

As the universe expands, the first scales to avoid damping are  $M \approx M_{JX_{\max}}$ , and then the condition (5.17a) will be fulfilled by successively shorter and shorter scales.

In the hot scenario, scales  $M \approx M_{JX_{\max}}$  have the longest time to grow, so that at recombination time  $T_R$ , the disturbance in the hot component will be preferentially on scales  $M \approx M_{JX_{\max}}$ .

Disturbances in the X gas may induce, for  $T < T_R$ , fluctuations in the baryonic component on scales

$$M_B = \frac{\Omega_B}{\Omega_X} M_{JX_{\max}} \quad (5.31)$$

which possibly are  $< M_c$  (see eq. (5.10)). In this case,  $M_{JX_{\max}}$  gives the scale of the first bound objects formed in the universe. For hot X particles, it is a supercluster scale: these are the first structures to appear, galaxies result from their fragmentation (pancake scenario (21)).

In warm and cold scenarios, on the contrary, the first scales to go non-linear are the smallest ones and large scale structures will develop as a result of hierarchical clustering of smaller structures (bottom-top picture, as for isothermal fluctuations).

## 5.2 OBSERVATIONS

Observational information on the large scale structure of the universe essentially consists of: i) the possible CMB anisotropy at small and large scales, ii) the clustering properties of the large scale distribution of galaxies which traces the light distribution in the universe, and iii) the large scale streaming motions.

Let us now consider them in turn.

i) Except for the possible detection of fluctuations on scales of  $8^\circ$  and  $6^\circ$ , CMB anisotropies have not yet been detected at small scales, only upper limits are available (see Chapter 3). This fact strongly constrains the viable scenarios for large scale structure formation. The strongest restriction is provided by the Usón and Wilkinson bound for arc min scales. But if reionization takes place at galaxy formation, then any imprint of density perturbations is erased on scales  $\lesssim 5^\circ$  and, in this case, the result on scales of  $8^\circ$  is the main constraint to large scale structure formation scenarios.

ii) Two methods are employed to find out the cosmic distribution of light:

a) The morphological analysis, which consists in looking for the shapes formed by the distribution of galaxies at scales of  $10-100 h^{-1}$  Mpc, by measuring the positions and (since a few years ago) red-shifts of selected galaxy samples. It became evident that light is not uniformly distributed in space at these scales. Galaxies appear to

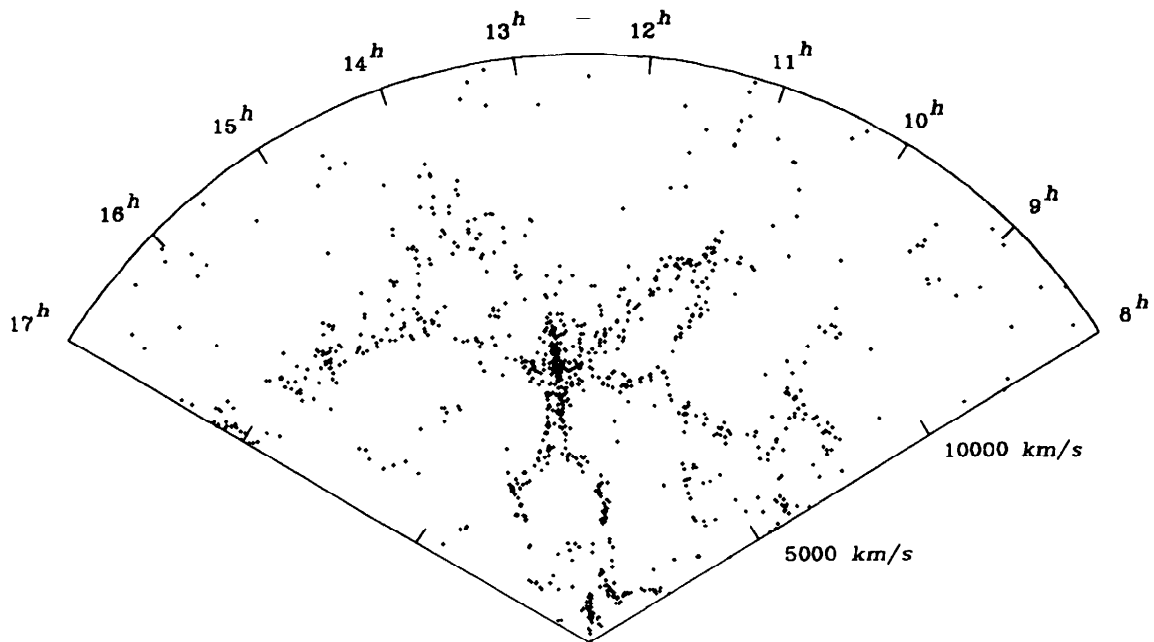


*Figure 5.3 Map of the red-shifts observed by de Lapparent et al. plotted versus right ascension in the declination wedge  $26^{\circ}.5 \leq \delta \leq 32^{\circ}.5$ . The objects plotted have  $m_B \leq 15.5$  and  $V \leq 15,000 \text{ km s}^{-1}$  (from de Lapparent, Geller and Huchra (23); published by the University of Chicago Press; copyright 1986 by the AAS).*

be clustered forming groups and clusters of different richnesses, often joined by filaments of length of about 50-100 Mpc. The three dimensional distribution, available to some extent after red-shift surveys, seems to suggest the presence of large voids, like the void in Boötes<sup>(22)</sup> or the regions devoid of bright galaxies found by de Lapparent et al. (1986)<sup>(23)</sup> in the Coma region, which have a diameter as large as  $30-50 \text{ h}^{-1} \text{ Mpc}$  (see figure 5.3). One must be aware, however, that some biases could be present in the samples<sup>(24)</sup>.

b) The statistical language is used to quantify the subjective

impression of clustering at different scales given by the galaxy distribution.

The most fruitful statistical method up to now has been the correlation function approach mainly developed by P.J.E. Peebles and co-workers<sup>(11,25)</sup> at Princeton. Its basic element is the two-point correlation function of cosmic objects (galaxies, clusters..),  $\xi(r)$ , defined by the expression

$$dp(r) = n^2 [1+\xi(r)] dv_1 dv_2 \quad (5.32)$$

where  $dp(r)$  is the joint probability of finding two objects in volumes  $dv_1$  and  $dv_2$  separated by a distance  $r$ ;  $n$  is the mean number density of the considered objects. (In eq. (5.32) it is implicitly assumed that the fluctuation field is homogeneous and isotropic). If the objects were uniformly or Poisson distributed, we would have  $\xi(r)=0$  and

$$dp(r) = n^2 dv_1 dv_2$$

From the catalogues of the projected distribution, one can get the two-point angular correlation function  $\omega(\theta)$ , defined by analogy with (5.32) by

$$dp(\theta) = N^2 [1 + \omega(\theta)] d\Omega_1 d\Omega_2 \quad (5.33)$$

where, now,  $dp(\theta)$  is the joint probability of finding two objects in the solid angle elements  $d\Omega_1$  and  $d\Omega_2$ , around directions separated by an angle  $\theta$ , and  $N$  is the projected number density of objects.  $\omega(\theta)$  and  $\xi(r)$  are related by Limber's formula<sup>(26)</sup>: